

Simplex Clustering via sBeta with Applications to Online Adjustment of Black-Box Predictions

Florent Chiaroni, Malik Boudiaf, Amar Mitiche and Ismail Ben Ayed

Abstract—We explore clustering the softmax predictions of deep neural networks and introduce a novel probabilistic clustering method, referred to as k -SBETAS. In the general context of clustering discrete distributions, the existing methods focused on exploring distortion measures tailored to simplex data, such as the KL divergence, as alternatives to the standard Euclidean distance. We provide a general maximum a posteriori (MAP) perspective of clustering distributions, emphasizing that the statistical models underlying the existing distortion-based methods may not be descriptive enough. Instead, we optimize a mixed-variable objective measuring data conformity within each cluster to the introduced sBeta density function, whose parameters are constrained and estimated jointly with binary assignment variables. Our versatile formulation approximates various parametric densities for modeling simplex data and enables the control of the cluster-balance bias. This yields highly competitive performances for the unsupervised adjustment of black-box model predictions in various scenarios. Our code and comparisons with the existing simplex-clustering approaches and our introduced softmax-prediction benchmarks are publicly available: https://github.com/fchiaroni/Clustering_Softmax_Predictions.

Index Terms—Probability simplex clustering, softmax predictions, deep black-box models, pre-trained, unsupervised adaptation.

1 INTRODUCTION

OVER the last decade, deep neural networks have continuously gained wide interest for the semantic analysis of real-world data. However, under real-world conditions, potential shifts in the feature or class distributions may affect the prediction performances of the pre-trained source models. To address this issue, several recent adaptation studies investigated fine-tuning all or a part of the model’s parameters using standard gradient-descent and back-propagation procedures [1], [2], [3]. However, in a breadth of practical applications, e.g., real-time predictions, it might be cumbersome to perform multiple forward and backward passes. This is particularly true when dealing with large (and continuously growing) pre-trained networks, such as the recently emerging foundational vision-language models [4]. In such scenarios, even fine-tuning only parts of the pre-trained model, such as the parameters of the normalization layers [1], might be computationally intensive. In addition, the existing adaptation techniques assume knowledge of the source model and its training procedures. Such assumptions may not always hold in practice due to data-privacy constraints [5] and the fact that many large-scale pre-trained models are only available through APIs [6], i.e., their pre-trained weights are not shared¹. Therefore, model-agnostic solutions, which enable computationally efficient adaptation of black-box pre-trained models, would be of

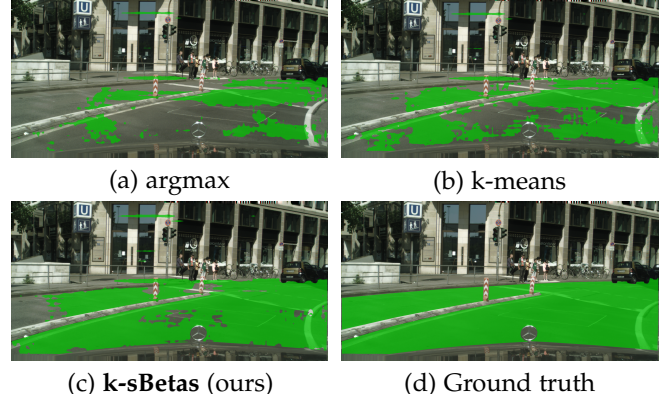


Fig. 1: **Real-time** (45 fps) black-box adaptation for road segmentation on images of size 2048×1024 by clustering the softmax predictions from a source model, pre-trained on GTA5 and applied to Cityscapes. See details in Sec. 5.3.

significant interest in practice.

In this work, we propose to cluster the softmax predictions of deep neural networks. Solely based on the model’s probabilistic outputs, this strategy yields computationally efficient adaptation while preserving the privacy of both the model and data. Fig. 1 depicts an application example for road segmentation under domain shifts.

Clustering the softmax output predictions of deep networks can be formulated as a clustering problem on the probability simplex domain, i.e., clustering discrete distributions. Probability simplex clustering is not a new problem and has been the subject of several early studies in other application domains such as text analysis [7], [8], [9], [10]. However, in the context of deep learning, clustering methods have been typically applied on deep feature maps, as in self-training frameworks [11]. This requires access to the internal feature maps of the source models, thereby violating the black-box assumption. In contrast, simplex-clustering-

• *F. Chiaroni was with ETS Montreal and INRS, Montreal, QC, Canada during this work and is now with Thales Research and Technology (TRT) Canada, Thales Digital Solutions (TDS), CortAIx, Montreal, QC, Canada. E-mail: florent.chiaroni.ai@gmail.com*

• *M. Boudiaf is with ETS Montreal, Montreal, QC, Canada. E-mail: malik.boudiaf.1@etsmtl.net*

• *A. Mitiche is with INRS, Montreal, QC, Canada. E-mail: Amar.Mitiche@inrs.ca*

• *I. Ben Ayed is with ETS Montreal, Montreal, Canada. E-mail: Ismail.BenAyed@etsmtl.ca*

1. This is the case, for instance, of large-scale foundation models in NLP such as the GPT family, Anthropic’s Claude or Google’s PaLM.

based adjustment of the probabilistic outputs of a deep pre-trained model complies with the black-box assumption but has remained largely under-explored, to the best of our knowledge.

The simplex clustering literature is often based on optimizing *distortion-based* objectives. The goal is to minimize, within each cluster, some distortion measure evaluating the discrepancy between a cluster representative and each sample within the cluster. Besides standard objectives like K-MEANS, which correspond to an $\|\cdot\|_2$ distortion, several simplex-clustering methods motivated and used distortion measures that are specific to simplex data. This includes, for instance, the Kullback-Leibler (KL) divergence [9], [10] and the Hilbert geometry distance [12]. In this work, we explore a general maximum a posteriori (MAP) perspective of clustering discrete distributions. Using the Gibbs model, we emphasize that the density functions underlying current distortion-based objectives (Table 1) may not properly approximate the empirical marginal distributions of real-world softmax predictions.

Fig. 2 illustrates our empirical observations through histograms representing the marginal (per-coordinate) distributions of real softmax predictions. These predictions were obtained using a black-box source model applied to data from an unseen target domain. We juxtapose these empirical histograms to parametric density functions estimated on the same predictions via various clustering methods. For instance, curve $p(Eucl)$ represents the parametric Gibbs model corresponding to the Euclidean distance used in K-MEANS. A close matching between the shape of the parametric density function and the one of the empirical histogram indicates a good fit of the simplex predictions. However, a significant disparity implies that the assumed parametric density function may not effectively model these predictions. For example, in Fig. 2 (c), the modes of parametric functions \mathcal{N} , $p(Eucl)$, $p(KL)$ and $p(HG)$ do not correspond to the one of the empirical distribution depicted with the orange histogram. Furthermore, Fig. 2 (d) depicts a particular scenario with an approximately uniform empirical distribution. In such cases, it is crucial for clustering models to generate unimodal density functions in order to preserve the assumption that the distribution of each class is unimodal. This avoids erroneously fitting multiple unimodal distributions to the data within a single cluster. As depicted in Fig. 2 (d), the standard Beta density may generate a bimodal distribution, thereby violating the unimodality assumption.

Contributions. Driven by the above observations, we introduce a novel probabilistic clustering objective integrating a generalization of the Beta density, which we coin **sBeta**. We derive several properties of **sBeta**, which enable us to impose different constraints on our clustering model, referred to as **K-SBETAS**, enforcing uni-modality of the densities within each cluster while avoiding degenerate solutions. We proceed with a block-coordinate descent approach, alternating optimization w.r.t assignment variables, and inner Newton iterations for solving the non-linear optimality conditions w.r.t the **sBeta** parameters. Furthermore, using the density moments, we derive a closed-form alternative to Newton iterations for parameter estimation. Our versatile formulation approximates various parametric densities for

modeling simplex data, including highly peaked distributions at the vertices of the simplex, as observed empirically in the case of deep-network predictions. It also enables the control of the cluster balance. We report comprehensive experiments, comparisons, and ablation studies, which show highly competitive performances of our simplex clustering for unsupervised adjustment of black-box predictions in a variety of scenarios. Fig. 2 illustrates the ability of our method to consistently fit the empirical marginal distributions of real-world softmax predictions. For instance, Fig. 2 (c) shows that the density peak of **sBeta** (orange curve) matches the highest bar of the histogram, enabling a more accurate fitting than the other methods. In addition, unlike the standard Beta density, our approach deliberately avoids fitting bimodal distributions (Fig. 2 (d)), thereby preventing degenerate solutions. This refinement not only ensures a more accurate representation of real data, but also maintains the assumption that the distribution of each class is unimodal. To reproduce our comparative experiments, we have made the codes publicly available, including the proposed **K-SBETAS** model, the explored state-of-the-art approaches, as well as the introduced softmax prediction benchmarks².

2 PROBLEM FORMULATION

We start by introducing the basic notations, which will be used throughout the article:

- $\Delta^{D-1} = \{\mathbf{x} \in [0, 1]^D \mid \mathbf{x}^T \mathbf{1} = 1\}$ stands for the $(D-1)$ -probability simplex.
- $\mathcal{X} = \{\mathbf{x}_i\}_{i=1}^N \stackrel{\text{iid}}{\sim} X$, with \mathcal{X} a given data set and X denoting the random simplex vector in Δ^{D-1} .
- $\mathcal{X}_k = \{\mathbf{x}_i \in \mathcal{X} \mid u_{i,k} = 1\}$ denotes cluster k , where $\mathbf{u}_i = (u_{i,k})_{1 \leq k \leq K} \in \Delta^{K-1} \cup \{0, 1\}$ is a latent binary vector assigning point \mathbf{x}_i to cluster k : $u_{i,k} = 1$ if \mathbf{x}_i belongs to cluster k and $u_{i,k} = 0$ otherwise. Let $\mathbf{U} \in \{0, 1\}^{NK}$ denote the latent assignment matrix whose column vectors are given by \mathbf{u}_i . Note that $\mathcal{X} = \mathcal{X}_1 \cup \dots \cup \mathcal{X}_{|\mathcal{Y}|}$.

Clustering consists of partitioning a given set \mathcal{X} into K different subsets \mathcal{X}_k referred to as clusters. In general, this is done by optimizing some objective functions with respect to the latent assignment variables \mathbf{U} . Often, the basic assumption underlying objective functions for clustering is that data points belonging to the same cluster k should be relatively close to each other, according to some pre-defined notion of closeness (e.g., via some distance or distortion measures).

In this study, we tackle the clustering of probability simplex data points (or distributions), with a particular focus on the output predictions from deep-learning models. Softmax³ is commonly used as the last activation function of neural-network classifiers to produce such output probability distributions. Each resulting softmax data point \mathbf{x} is a D -dimensional probability vector of D continuous random variables, which are in $[0, 1]$ and sum to one. Thus, the

2. https://github.com/fchiaroni/Clustering_Softmax_Predictions

3. Also referred to as the normalized exponential function, the softmax function is defined as $\sigma(\mathbf{z})_j = \frac{\exp(z_j)}{\sum_{l=1}^D \exp(z_l)}$, with $\mathbf{z} = \{z_1, \dots, z_D\}$ denoting a vector of logits.

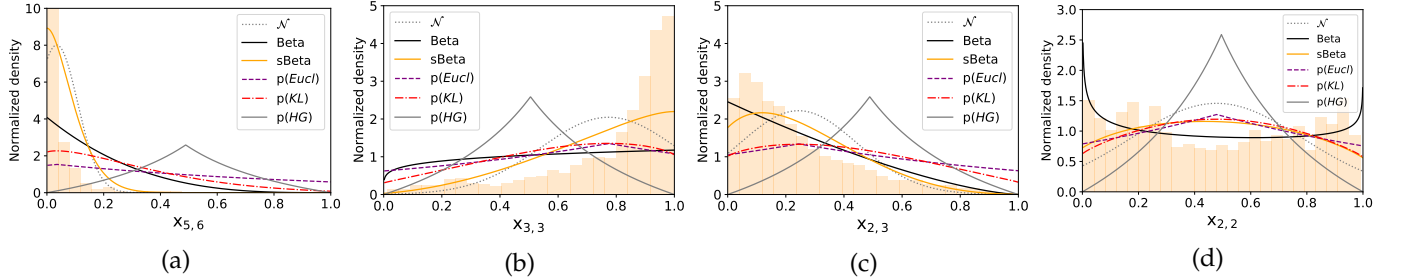


Fig. 2: **Modelling softmax marginal distributions.** Figures (a), (b), (c) and (d) compare the density fittings of real-world marginal distributions of softmax predictions, represented by their respective histograms (orange bars). Specifically, the histograms in Fig. (a), (b), and (d) were extracted from the SVHN \rightarrow MNIST benchmark and the one in (c) from the VISDA-C one (details in Sec. 5.1.2). Figs. 8 and 9 in the Appendix depict the whole set of histograms per class. Normalized probability density functions \mathcal{N} , $p(Eucl)$, $p(KL)$, $p(HG)$, Beta and sBeta are obtained, respectively, from the normal density, Euclidean distance, Kullback-Leibler divergence, Hilbert distance, Beta, and sBeta, all listed in Table. 1.

target clustering challenge is defined on probability simplex domain Δ^{D-1} . Fig. 3 depicts mixtures of three class distributions on Δ^2 , simulating the impact of a domain shift on the softmax predictions, as well as the benefits of simplex clustering over the standard argmax prediction in such a scenario. Specifically, Fig. 3 (a) shows the softmax predictions from a model trained on and applied to the same source domain. In this case, the standard argmax function, commonly used in deep networks, effectively separates the three classes. In contrast, Fig. 3 (b) reveals that, in the case of a domain shift, the argmax function may lead to erroneous predictions. Fig. 3 (c) illustrates how a simplex clustering successfully maintains class cohesion in this case. This synthetic example points to the potential of simplex clustering in dealing with domain-shift challenges while operating solely on the outputs (i.e., in a black-box setting).

3 RELATED WORK

This section presents related work in the general context of clustering, focusing on the probability simplex domain.

3.1 Distortion-based clustering objectives

The most widely used form of clustering objectives is based on some *distortion* measures, for instance, a distance in general-purpose clustering or a divergence measure in the case of probability simplex data. This amounts to minimizing w.r.t both assignment variables and cluster representatives $\Theta = (\theta_k)_{1 \leq k \leq K}$ a mixed-variable function of the following general form:

$$L_{dist}(\mathbf{U}; \Theta) = \sum_{k=1}^K \sum_{i=1}^N u_{i,k} \|\mathbf{x}_i - \theta_k\|_d = \sum_{k=1}^K \sum_{\mathbf{x}_i \in \mathcal{X}_k} \|\mathbf{x}_i - \theta_k\|_d.$$

The goal is to minimize, within each cluster \mathcal{X}_k , some distortion measure $\|\cdot\|_d$ evaluating the discrepancy between cluster representative θ_k and each point belonging to the cluster. When $\|\cdot\|_d$ is the Euclidean distance, general form (1) becomes the standard and widely used K-MEANS objective [13]. In general, optimizing distortion-based objective (1) is NP-hard⁴. One standard iterative solution to tackle the

4. For example, a proof of the NP-hardness of the standard K-MEANS objective could be found in [14].

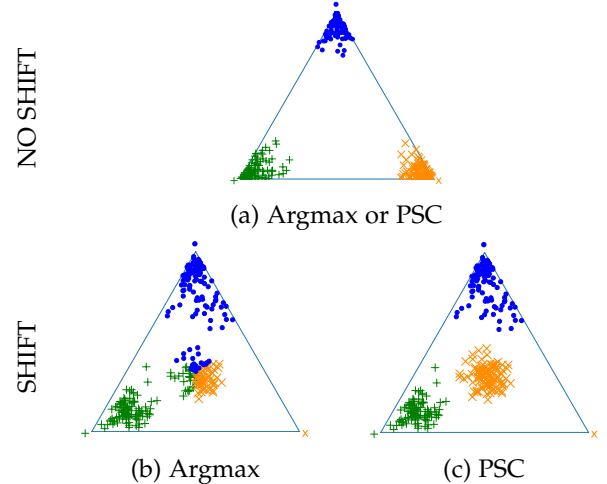


Fig. 3: **Partitioning points within probability simplex Δ^2 .** Specifically, these points are projected into a 2D equilateral triangle for a clear visualization, where each vertex represents one dimension of the probability space. The figures depict the probabilistic predictions from a hypothetical source model, with and without distribution shift. Fig. (b) depicts the standard argmax assignment, whereas Fig. (c) represents a Probability Simplex Clustering (PSC) using a cluster-to-class alignment. Symbols + (green), x (orange) and • (blue) indicate separate class assignments.

problem in (1) is to follow a block-coordinate descent approach, which alternates two steps, one optimizes the objective w.r.t to the cluster prototypes and the other w.r.t assignment variables:

- **U-update:** $u_{i,k} = \begin{cases} 1 & \text{if } \arg \min_k \|\mathbf{x}_i - \theta_k\|_d = k \\ 0 & \text{otherwise.} \end{cases}$
- **Θ -update:** Find $\arg \min_{\Theta} L_{dist}(\mathbf{U}; \Theta)$

In the specific case of K-MEANS (i.e., using the $\|\cdot\|_2$ distance as distortion measure), optimization w.r.t the parameters in the Θ -update step yields closed-form solutions, which correspond to the *means* of features within the clusters:

$$\theta_k = \frac{\sum_{i=1}^N u_{i,k} \mathbf{x}_i}{\sum_{i=1}^N u_{i,k}}, \forall k.$$

One way to generalize K-MEANS is to replace the Euclidean distance with other distortion measures. In this case, the optimal value of the parameters θ_k may no longer correspond to cluster means. For instance, when using the $\|\cdot\|_1$ distance as distortion measure in (1), the optimal θ_k corresponds to the cluster median, and the ensuing algorithm is the well-known K-MEDIAN clustering [15]. For exponential distortions, the optimal parameters may correspond to cluster modes [16], [17]. Such exponential distortions enable the model to be more robust to outliers, but this comes at the price of additional computations (inner iterations), as cluster modes could not be obtained in closed-form.

3.2 Distortion measures for simplex data

In our case, data points are probability vectors within simplex domain Δ^{D-1} , e.g. the softmax predictions of deep networks. These points are D -dimensional vectors of D continuous random variables bounded between 0 and 1, and summing to one. To our knowledge, the simplex clustering literature is often based on distortion objectives of the general form in (1). Besides standard objectives like K-MEANS, several simplex-clustering works motivated and used distortion measures that are specific to simplex data. This includes the Kullback-Leibler (KL) divergence [9], [10] and Hilbert geometry distance [12].

Information-theoretic k-means. The works in [9], [10] discussed **KL K-MEANS**, a distortion-based clustering tailored to simplex data and whose objective fits the general form in (1). KL K-MEANS uses the Kullback-Leibler (KL) divergence as a distortion measure instead of the Euclidean distance in the standard K-MEANS:

$$\|\mathbf{x}_i - \boldsymbol{\theta}_k\|_d = \text{KL}(\mathbf{x}_i || \boldsymbol{\theta}_k) = \sum_{n=1}^D x_{i,n} \log \left(\frac{x_{i,n}}{\theta_{k,n}} \right), \quad (2)$$

where $x_{i,n}$ and $\theta_{k,n}$ stand, respectively, for the n -th component of simplex vectors \mathbf{x}_i and $\boldsymbol{\theta}_k$. $\text{KL}(\mathbf{x}_i || \boldsymbol{\theta}_k)$ is a Bregman divergence [8] measuring the dissimilarity between two distributions \mathbf{x}_i and $\boldsymbol{\theta}_k$. Despite being asymmetric [10], the machine learning community widely uses the KL divergence in a breadth of problems where one has to deal with probability simplex vectors [18], [19], [20], [21].

Hilbert Simplex Clustering (HSC). More recently, the study in [12] investigated the Hilbert Geometry (HG) distortion with *minimum enclosing ball* (MEB) centroids [22], [23] for clustering probability simplex vectors. For a given cluster set k , the MEB center represents the midpoint of the two farthest points within the set. Given two points \mathbf{x}_i and $\boldsymbol{\theta}_k$ within simplex domain Δ^{D-1} , let $\mathbf{x}_i + t(\boldsymbol{\theta}_k - \mathbf{x}_i)$, $t \in \mathbb{R}$, denote the line passing through points \mathbf{x}_i and $\boldsymbol{\theta}_k$, with $t_0 \leq 0$ and $t_1 \geq 1$ the two intersection points of this line with the simplex domain boundary $\partial\Delta^{D-1}$. Then, HG simplex distortion is given by:

$$\begin{aligned} \text{HG}_{\Delta^{D-1}}(\mathbf{x}_i; \boldsymbol{\theta}_k) &= \left| \log \left(\frac{(1-t_0)t_1}{(-t_0)(t_1-1)} \right) \right| \\ &= \log \left(1 - \frac{1}{t_0} \right) - \log \left(1 - \frac{1}{t_1} \right). \end{aligned} \quad (3)$$

Note that if one deals with centroids close or equal to the vertices of the simplex, then HG distortion would inconsistently output large or infinite distance values near such centroids.

3.3 From distortions to probabilistic clustering

Beyond distortions, a more versatile approach is to minimize the following well-known maximum a posteriori (MAP) generalization of K-MEANS [24], [25], [26], coined by [26] as *probabilistic K-MEANS*:

$$L_{\text{prob}}(\mathbf{U}; \boldsymbol{\pi}; \boldsymbol{\Theta}) = - \sum_{k=1}^K \sum_{i=1}^N u_{i,k} \log(\pi_k f(\mathbf{x}_i; \boldsymbol{\theta}_k)), \quad (4)$$

where $f(\cdot; \boldsymbol{\theta}_k)$ is a parametric density function modeling the likelihood probabilities of the samples within cluster k , and π_k the prior probability of cluster k , with $\boldsymbol{\pi} = (\pi_k)_{1 \leq k \leq K} \in \Delta^{K-1}$. Hence, instead of minimizing a distortion $\|\mathbf{x}_i - \boldsymbol{\theta}_k\|_d$ in (1), we maximize a more general quantity measuring the posterior probability of cluster k given sample \mathbf{x}_i and parameters $\boldsymbol{\theta}_k$. It is easy to see that, for any choice of distortion measure, the objective in (1) corresponds, up to a constant, to a particular case of probabilistic K-MEANS in (4), with $\pi_k = 1/K, \forall k$, and parametric density f chosen to be the *Gibbs* distribution:

$$f(\mathbf{x}_i; \boldsymbol{\theta}_k) \propto \exp(-\|\mathbf{x}_i - \boldsymbol{\theta}_k\|_d). \quad (5)$$

For instance, the K-MEANS objective corresponds, up to additive and multiplicative constants, to choosing likelihood probability $f(\mathbf{x}_i; \boldsymbol{\theta}_k)$ to be a Gaussian density with mean equal to $\boldsymbol{\theta}_k$, identity covariance matrix and prior probabilities verifying $\pi_k = 1/K, \forall k$. This uncovers hidden assumptions in K-MEANS: The samples are assumed to follow Gaussian distribution within each cluster, and the clusters are assumed to be balanced⁵. Therefore, the general probabilistic K-MEANS formulation in (4) is more versatile as it enables to make more appropriate assumptions about the parametric statistical models of the samples within the clusters (e.g., via prior knowledge or validation data), and to manage the cluster-balance bias [24].

3.4 Do current simplex clustering methods model softmax predictions properly?

Eq. (5) emphasized that there are implicit density functions underlying distortion-based clustering objectives via Gibbs models; see Table 1. Fig. 2 illustrates how the Gibbs models corresponding to the existing simplex clustering algorithms may not properly approximate the empirical marginal density functions of real-world softmax predictions:

Standard K-MEANS: Fast, but not descriptive enough and biased. The well-known K-MEANS clustering falls under the probabilistic clustering framework, as defined in Sec. 3.3. In particular, it instantiates the data likelihoods as Gaussian densities with unit covariance matrices. An important advantage of K-MEANS is that the associated $\boldsymbol{\Theta}$ -update step can be analytically solved by simply updating each θ_k as the mean of samples within cluster k , according to the current latent assignments. Such closed-form solutions enable K-MEANS to be among the most efficient clustering algorithms. However, the Gaussian assumption yielding such closed-form solutions might be limiting when dealing with asymmetric data densities, such as exponential densities, with the particularity that the mode and the mean are distinct. As

5. In fact, it is well-known that K-MEANS has a strong bias towards balanced partitions [24]

TABLE 1: Comparison of metrics and density functions, depending on the probability simplex vector $\mathbf{x}_i = (x_{i,n})_{1 \leq n \leq D} \in \Delta^{D-1}$ and the parameters $\boldsymbol{\theta}_k = (\theta_{k,n})_{1 \leq n \leq D}$ for Euclidean, KL, and $HG_{\Delta^{D-1}}$ distortions. $\boldsymbol{\theta}_k$ respectively represents the density parameters $\boldsymbol{\theta}_k = (\boldsymbol{\mu}_k, \boldsymbol{\Sigma}_k)$ with $\boldsymbol{\mu}_k = (\mu_{k,n})_{1 \leq n \leq D}$ for \mathcal{N} , $\boldsymbol{\theta}_k = (\alpha_{k,n})_{1 \leq n \leq D}$ for f_{Dir} , and $\boldsymbol{\theta}_k = (\alpha_{k,n}, \beta_{k,n})_{1 \leq n \leq D}$ for g_{Beta} and g_{sBeta} .

METRIC-BASED	$\exp(-\text{METRIC}(\mathbf{x}_i; \boldsymbol{\theta}_k))$
$\ \mathbf{x}_i - \boldsymbol{\theta}_k\ _2$	$\exp\left(-\sqrt{\sum_{n=1}^D (x_{i,n} - \theta_{k,n})^2}\right)$
$\text{KL}(\mathbf{x}_i \boldsymbol{\theta}_k)$	$\prod_{n=1}^D \exp\left(-x_{i,n} \cdot \log \frac{x_{i,n}}{\theta_{k,n}}\right)$
$HG_{\Delta^{D-1}}(\mathbf{x}_i; \boldsymbol{\theta}_k)$ (Eq. (3))	$(1 - \frac{1}{t_1})/(1 - \frac{1}{t_0})$

PROBABILISTIC	$f(\mathbf{x}_i; \boldsymbol{\theta}_k)$
$\mathcal{N}(\mathbf{x}_i; \boldsymbol{\theta}_k)$	$\frac{1}{\sqrt{(2\pi)^n \Sigma_k }} \exp\left(-\frac{1}{2} (\mathbf{x}_i - \boldsymbol{\mu}_k)^T \Sigma_k^{-1} (\mathbf{x}_i - \boldsymbol{\mu}_k)\right)$
$f_{\text{Dir}}(\mathbf{x}_i; \boldsymbol{\theta}_k)$	$\frac{\prod_{n=1}^D x_{i,n}^{(\alpha_{k,n}-1)}}{B(\boldsymbol{\theta}_k)}$
$g_{\text{Beta}}(\mathbf{x}_i; \boldsymbol{\theta}_k)$	$\prod_{n=1}^D \frac{(x_{i,n})^{\alpha_{k,n}-1} (1 - x_{i,n})^{\beta_{k,n}-1}}{B(\alpha_{k,n}, \beta_{k,n})}$
$g_{\text{sBeta}}(\mathbf{x}_i; \boldsymbol{\theta}_k)$	$\prod_{n=1}^D \frac{(x_{i,n} + \delta)^{\alpha_{k,n}-1} (1 + \delta - x_{i,n})^{\beta_{k,n}-1}}{B(\alpha_{k,n}, \beta_{k,n}) (1 + 2\delta)^{\alpha_{k,n} + \beta_{k,n} - 2}}$

depicted by Fig. 2 (a) and (b), the softmax outputs from actual deep-learning models commonly follow such asymmetric distributions. Note that K-MEANS and other distortion-based objectives correspond to setting $\pi_k = 1/K, \forall k$ in the general probabilistic formulation in Eq. (4). Therefore, they encode the implicit strong bias towards balanced partitions [24], and might be sub-optimal when dealing with imbalanced clusters, as is often the case of realistic deep-network predictions.

Elliptic K-MEANS. Elliptic K-MEANS is a generalization of the standard K-means: It uses the Mahalanobis distance instead of the Euclidean distance, which assumes the data within each cluster follows a Gaussian distribution (i.e. Gibbs model for the Mahalanobis distance) whose covariance matrix is also a variable of the model (as opposed to unit covariance in K-MEANS); see Table 1. Fig. 2 (b) and (c) confirm that Gaussian density function \mathcal{N} is not appropriate for skewed distributions, as is the case of network predictions.

HSC yields poor approximations of highly peaked distributions located at the vertices of the simplex. Fig. 2 shows that HSC, which combines MEB centroids and HG metric, is not relevant to asymmetric distributions whose modes are close to the vertices of the simplex. Specifically, in Fig. 2 (a) and (b), the corresponding Gibbs probability is small near the vertices of the simplex and high in the middle of the simplex. This yields a poor approximation of the target empirical histograms (depicted in orange). In addition, the overall HSC algorithm is computationally demanding (see Table. 3).

KL K-MEANS. While KL could yield asymmetric density, it may poorly model highly peaked distributions at the

vertices of the simplex (e.g. Fig. 2 a), as is the case of softmax predictions.

4 PROPOSED APPROACH

4.1 Background

Multivariate Dirichlet density function: Commonly used for modeling categorical events, the Dirichlet density operates on D -dimensional discrete distributions within the simplex, Δ^{D-1} . Its expression, parameterized by vector $\boldsymbol{\alpha} = (\alpha_n)_{1 \leq n \leq D} \in \mathbb{R}^D$, is given by:

$$f_{\text{Dir}}(\mathbf{x}; \boldsymbol{\alpha}) = \frac{1}{B(\boldsymbol{\alpha})} \prod_{n=1}^D x_n^{\alpha_n-1}, \quad (6)$$

with $\mathbf{x} \in \Delta^{D-1}$, and $B(\boldsymbol{\alpha})$ the multivariate Beta function expressed using the Gamma function⁶. While the Dirichlet density is designed for simplex vectors, its complex nature leads to computationally intensive optimization, often involving iterative and potentially sub-optimal parameter estimation [27]. To address this computational challenge, one could adopt the mean-field approximation principle [28]. This uses a relaxed product density, which is based on Dirichlet's marginal density, i.e. Beta with parameters $\boldsymbol{\alpha}$ and $\boldsymbol{\beta}$:

$$\begin{aligned} g_{\text{Beta}}(\mathbf{x}; \boldsymbol{\alpha}, \boldsymbol{\beta}) &= \prod_{n=1}^D f_{\text{Beta}}(x_n; \alpha_n, \beta_n) \\ &= \prod_{n=1}^D \frac{(x_n)^{\alpha_n-1} (1 - x_n)^{\beta_n-1}}{B(\alpha_n, \beta_n)} \\ &\approx f_{\text{Dir}}(\mathbf{x}; \boldsymbol{\alpha}). \end{aligned} \quad (7)$$

This approximation simplifies parameter estimation by treating each simplex coordinate independently. However, apart from the computational load, Dir and its marginal Beta may yield poor approximations of the empirical marginal distributions of real-world softmax predictions. For example, Fig. 2 (a), (b), and (c) show how Beta has difficulty capturing empirical marginal distributions. In addition, Dir allows multimodal distributions, as shown with its Beta marginal in Fig. 2 (d), opposing the common assumption that each semantic class distribution is unimodal. Indeed, discriminative deep learning models are optimized to output probability simplex vertices (i.e. one-hot vectors). For each class, the model is optimized to output softmax predictions following an unimodal distribution. In this context, Dir may erroneously represent two unimodal distributions as a single bimodal distribution.

In the next section, we propose sBeta, an alternative capable of effectively addressing these limitations.

4.2 Proposed density function: A generalization of Beta constrained to be unimodal

Unlike Beta, we seek a density function that can approximate highly peaked densities near the vertices of the simplex while satisfying a uni-modality constraint, thereby avoiding degenerate solutions and accounting for the statistical properties of real-world softmax predictions.

6. The Gamma function $\Gamma(\alpha) = \int_0^\infty t^{\alpha-1} \exp(-t) dt$ for $\alpha > 0$. $\Gamma(\alpha) = (\alpha - 1)!$ when α is a strictly positive integer.

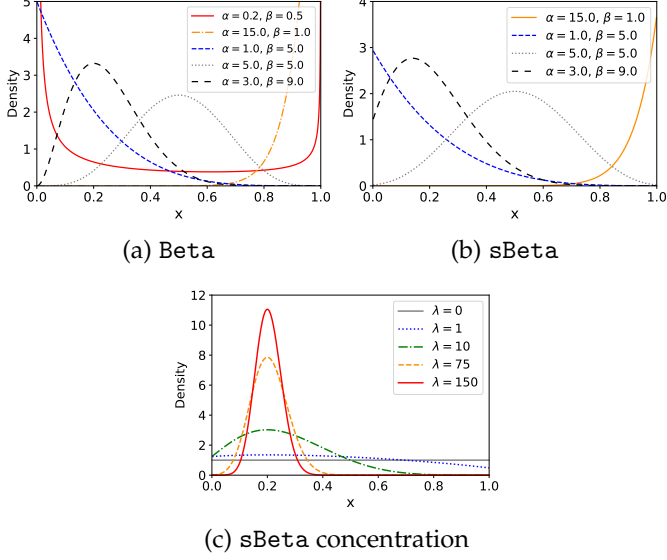


Fig. 4: Beta and sBeta density functions. Figures (a) and (b) respectively illustrate Beta density function, and the presented variant referred to as sBeta. Fig. (c) shows sBeta depending on the concentration parameter λ while maintaining the same mode.

4.2.1 Generalization of Beta

We propose the following generalization of Beta, which we refer to as sBeta (scaled Beta) in the sequel:

$$f_{\text{sBeta}}(x; \alpha, \beta) = \frac{(x + \delta)^{\alpha-1}(1 + \delta - x)^{\beta-1}}{B(\alpha, \beta)(1 + 2\delta)^{\alpha+\beta-2}}, \quad (8)$$

with $\delta \in \mathbb{R}^+$. Clearly, when parameter δ is set equal to 0, the generalization in (8) reduces to Beta density f_{Beta} in (7). Figures 4 (a) and (b) depict Beta and sBeta density functions for different values of parameters α and β , showing the difference between the two densities. For instance, for $\alpha = 3$ and $\beta = 9$, one may observe that sBeta is characterized by a higher density than Beta in the proximity of the simplex vertex in this particular example. As illustrated in Figs. 2 (a), (b) and (c), sBeta approximations of the empirical distributions (orange histograms) of the softmax predictions are better than those obtained with the Beta density. Overall, sBeta can be viewed as a scaled variant of Beta. It is relatively more permissive, enabling it to fit a wider range of unimodal simplex distributions.

In the following, we provide expressions of the moments (first and second central) and mode of sBeta as functions of density parameters α and β . As we will see shortly, these properties will enable us to integrate different constraints with our sBeta-based probabilistic clustering objective, enforcing uni-modality of the distribution within each cluster while avoiding degenerate solutions. Furthermore, they will enable us to derive a computationally efficient, moment-based estimation of the density parameters.

4.2.2 Mean and Variance

Property 1. The mean $E_{sB}[X]$ of sBeta could be expressed as a function of the density parameters as follows:

$$E_{sB}[X] = \frac{\alpha}{\alpha + \beta}(1 + 2\delta) - \delta. \quad (9)$$

Proof. The mean $E_{sB}[X]$ of sBeta could be found by integrating $xf_{\text{sBeta}}(x)$. A detailed derivation is provided in Appendix A. \square

Property 2. The variance $V_{sB}[X]$ of sBeta could be expressed as a function of the density parameters as follows:

$$V_{sB}[X] = \frac{\alpha\beta}{(\alpha + \beta)^2(\alpha + \beta + 1)}(1 + 2\delta)^2. \quad (10)$$

Proof. We use $V_{sB}[X] = E_{sB}[X^2] - E_{sB}[X]^2$, with $E_{sB}[X^2]$ denoting the second moment of sBeta, which could be found by integrating $x^2 f_{\text{sBeta}}(x)$. The details of the computations of $E_{sB}[X^2]$ and $V_{sB}[X]$ are provided in the Appendix. A. \square

4.2.3 Mode and Concentration

The mode of a density function $f(x)$ corresponds to the value of x at which $f(x)$ achieves its maximum.

Property 3. The mode m_{sB} of sBeta could be expressed as a function of the density parameters as follows:

$$m_{sB} = \frac{\alpha - 1 + \delta(\alpha - \beta)}{\alpha + \beta - 2}. \quad (11)$$

Proof. The mode m_{sB} of sBeta can be found by estimating at which value of x the derivative of f_{sBeta} is equal to 0. A detailed derivation can be found in Appendix A. \square

Note that, when $\alpha = \beta$, we have $m_{sB} = E_{sB}[X] = \frac{1}{2}$. Otherwise, $m_{sB} \neq E_{sB}[X]$. Thus, sBeta is asymmetric when $\alpha \neq \beta$, and the variance is consequently inadequate to measure the dispersion around sBeta mode.

Concentration parameter. Motivated by the previous observation, we present the concentration parameter λ to measure how much a sample set is condensed around the mode value. The concept of concentration parameter has been previously discussed in [29]. With respect to the mode equation 11, we express $\lambda = \alpha + \beta - 2$ such that we have

$$m_{sB} = \frac{\alpha - 1 + \delta(\alpha - \beta)}{\lambda}. \quad (12)$$

Using Eq. (12), we can express α and β as functions of the mode and concentration parameter:

$$\begin{cases} \alpha = 1 + \lambda \frac{m_{sB} + \delta}{1 + 2\delta} \\ \beta = 1 + \lambda \frac{1 + \delta - m_{sB}}{1 + 2\delta} \end{cases} \quad (13)$$

Fig. 4 (c) shows different concentrations around a given mode when changing λ .

4.3 Proposed clustering model: κ -sBETAS

Probabilistic clustering. We cast clustering distributions as minimizing the following probabilistic objective (κ -sBETAS), which measures the conformity of data within each cluster to a multi-variate sBeta density function, subject to constraints that enforce uni-modality and discourage degenerate solutions:

$$L_{\text{sBeta}}(\mathbf{U}; \boldsymbol{\pi}; \boldsymbol{\Theta}) = - \sum_{i=1}^N \sum_{k=1}^K u_{i,k} \log (\pi_k g_{\text{sBeta}}(\mathbf{x}_i; \boldsymbol{\alpha}_k, \boldsymbol{\beta}_k)) \quad (14)$$

$$\text{s.t. } \begin{cases} \lambda_{k,n} \geq \tau^- \forall k, n : \text{ Unimodal constraint, Sec. 4.3.2} \\ \lambda_{k,n} \leq \tau^+ \forall k, n : \text{ Avoids Dirac solutions, Sec. 4.3.2} \end{cases} \quad (15)$$

where g_{sBeta} is a multivariate extension of sBeta :

$$g_{\text{sBeta}}(\mathbf{x}_i; \boldsymbol{\alpha}_k, \boldsymbol{\beta}_k) = \prod_{n=1}^D f_{\text{sBeta}}(x_{i,n}; \alpha_{k,n}, \beta_{k,n}),$$

and $\lambda_{k,n}$ denotes the concentration parameter of univariate $f_{\text{sBeta}}(x_{i,n}; \alpha_{k,n}, \beta_{k,n})$. In our model in (14), $\boldsymbol{\Theta} = (\boldsymbol{\alpha}_k, \boldsymbol{\beta}_k)_{1 \leq k \leq K}$, with $\boldsymbol{\alpha}_k = (\alpha_{k,n})_{1 \leq n \leq D}$ and $\boldsymbol{\beta}_k = (\beta_{k,n})_{1 \leq n \leq D}$, $\boldsymbol{\pi} = (\pi_k)_{1 \leq k \leq K} \in \Delta^{K-1}$ and, following the general notation we introduced in Sec. 2, \mathbf{U} denotes binary point-to-cluster assignments.

4.3.1 Block-coordinate descent optimization

Our objective in (14) depends on three different sets of variables: \mathbf{U} ; $\boldsymbol{\pi}$; and sBeta parameters $\boldsymbol{\Theta}$. Therefore, we proceed with a block-coordinate descent approach, alternating three steps. Each step optimizes the objective w.r.t a set of variables while keeping the rest of the variables fixed.

- **$\boldsymbol{\Theta}$ updates, with \mathbf{U} and $\boldsymbol{\pi}$ fixed:** This section presents two different strategies for updating the sBeta parameters:

(a) *Solving the necessary conditions for the minimum of L_{sBeta} w.r.t $\alpha_{k,n}$ and $\beta_{k,n}$:*

Our objective in (14) is convex in each $\alpha_{k,n}$ and $\beta_{k,n}$. The global optima could be obtained by setting the gradient to zero. This could be viewed as a maximum likelihood estimation approach (MLE). Unfortunately, this yields a non-linear system of equations that, cannot be solved in closed-form. Therefore, we proceed to an inner iteration. In the appendix, we derive the following iterative and alternating updates to solve the non-linear system of equations:

$$\boldsymbol{\alpha}_k^{(t+1)} = \psi^{-1}(\psi(\boldsymbol{\alpha}_k^{(t)} + \boldsymbol{\beta}_k^{(t)}) + \frac{1}{\sum_{i=1}^N u_{i,k}} \sum_{i=1}^N u_{i,k} \log(\frac{x_i + \delta}{1 + 2\delta})) \quad (16)$$

$$\boldsymbol{\beta}_k^{(t+1)} = \psi^{-1}(\psi(\boldsymbol{\alpha}_k^{(t)} + \boldsymbol{\beta}_k^{(t)}) + \frac{1}{\sum_{i=1}^N u_{i,k}} \sum_{i=1}^N u_{i,k} \log(\frac{1 + \delta - x_i}{1 + 2\delta})) \quad (17)$$

where t refers to iteration number and ψ corresponds to the digamma function. Note that neither ψ nor ψ^{-1} admit analytic expressions. Instead, we follow [27] to approximate those functions, at the cost of additional Newton iterations. The full derivation of the updates and all required details could be found in the Appendix.

(b) *Method of moments (MoM):*

As a computationally efficient alternative to solving a non-linear system within each outer iteration, we introduce an approximate estimation of sBeta parameters $\boldsymbol{\alpha}_k$ and $\boldsymbol{\beta}_k$, which we denote $\boldsymbol{\alpha}_k$ and $\boldsymbol{\beta}_k$, as

the solutions to the first and second central moment equations, following Prop. 1 and Prop. 2:

$$\begin{cases} \boldsymbol{\mu}_k &= \frac{\boldsymbol{\alpha}_k}{\boldsymbol{\alpha}_k + \boldsymbol{\beta}_k} (1 + 2\delta) - \delta \\ \mathbf{v}_k &= \frac{\boldsymbol{\alpha}_k \boldsymbol{\beta}_k}{(\boldsymbol{\alpha}_k + \boldsymbol{\beta}_k)^2 (\boldsymbol{\alpha}_k + \boldsymbol{\beta}_k + 1)} (1 + 2\delta)^2 \end{cases} \quad (18)$$

where $\boldsymbol{\mu}_k$ and \mathbf{v}_k denote, respectively, the empirical means and variances of cluster k :

$$\boldsymbol{\mu}_k = \frac{\sum_{i=1}^N u_{i,k} \mathbf{x}_i}{\sum_{i=1}^N u_{i,k}} \text{ and } \mathbf{v}_k = \frac{\sum_{i=1}^N u_{i,k} (\mathbf{x}_i - \boldsymbol{\mu}_k)^2}{\sum_{i=1}^N u_{i,k}}. \quad (19)$$

The system of two equations and two unknowns in (18) could be solved efficiently in closed-form, which yields the following estimates of sBeta parameters:

$$\begin{cases} \boldsymbol{\alpha}_k &= (\frac{\boldsymbol{\mu}_k^\delta (1 - \boldsymbol{\mu}_k^\delta) (1 + 2\delta)^2}{\mathbf{v}_k} - 1) \boldsymbol{\mu}_k^\delta \\ \boldsymbol{\beta}_k &= (\frac{\boldsymbol{\mu}_k^\delta (1 - \boldsymbol{\mu}_k^\delta) (1 + 2\delta)^2}{\mathbf{v}_k} - 1) (1 - \boldsymbol{\mu}_k^\delta) \end{cases} \quad (20)$$

with $\boldsymbol{\mu}_k^\delta = \frac{\boldsymbol{\mu}_k + \delta}{1 + 2\delta}$.

- **\mathbf{U} updates, with $\boldsymbol{\Theta}$ and $\boldsymbol{\pi}$ fixed:** With variables $\boldsymbol{\Theta}$ and $\boldsymbol{\pi}$ fixed, the global optimum of our objective in (14) with respect to assignment variables \mathbf{U} , subject to constraints $\mathbf{u}_i = (u_{i,k})_{1 \leq k \leq K} \in \Delta^{K-1} \cup \{0, 1\}$, corresponds to the following closed-form solution for each assignment variable $u_{i,k}$:

$$u_{i,k} = \begin{cases} 1 & \text{if } \arg \max_k \pi_k \cdot g_{\text{sBeta}}(\mathbf{x}_i; \boldsymbol{\alpha}_k, \boldsymbol{\beta}_k) = k \\ 0 & \text{otherwise.} \end{cases} \quad (21)$$

- **$\boldsymbol{\pi}$ updates, with \mathbf{U} and $\boldsymbol{\Theta}$ fixed:** Solving the Karush–Kuhn–Tucker (KKT) conditions for the minimum of (14) with respect to $\boldsymbol{\pi}$, s.t $\boldsymbol{\pi} \in \Delta^{K-1}$, yields the following closed-form solution for each π_k :

$$\pi_k = \frac{\sum_{i=1}^N u_{i,k}}{N}. \quad (22)$$

4.3.2 Handling parameter constraints

Our model in (14) integrates two constraints on concentration parameters $\lambda_{k,n}$; one discourages multi-modal solutions, and the other avoids degenerate, highly peaked (Dirac) densities.

Notice that the sBeta density is bimodal when $\alpha_{k,n} < 1$ and $\beta_{k,n} < 1$, which corresponds to $\lambda_{k,n} < 0$ (as $\lambda_{k,n} = \alpha_{k,n} + \beta_{k,n} - 2$). Moreover, setting $\alpha_{k,n} = \beta_{k,n} = 1$, which yields $\lambda_{k,n} = 0$, corresponds to the uniform density. Thus, to constrain the sBeta densities to be strictly unimodal, we must restrict $\lambda_{k,n}$ to positive values. In practice, we constrain $\lambda_{k,n}$ to be greater or equal to a threshold $\tau^- > 0$, which we simply set to 1.

A high-density concentration around the sBeta mode corresponds to high values $\lambda_{k,n}$. Thus, to avoid degenerate, highly peaked (Dirac) densities, we constrain $\lambda_{k,n}$ to stay smaller than or equal to a fixed, strictly positive threshold τ^+ .

Overall, we enforce $\tau^- \leq \lambda_{k,n} \leq \tau^+$ on sBetas parameters using Eq. (13), as detailed in Algorithm 1. This procedure allows for maintaining the same mode. Fig. 5 (a) shows sBeta density estimation, following the constraint $\lambda_{k,n} \geq \tau^-$, on a bimodal distribution sample. Fig. 5 (b) shows sBeta estimation, following the constraint $\lambda_{k,n} \leq \tau^+$, on a Dirac distribution sample.

Algorithm 1 Constraints for sBeta parameters

```

1: global variables
2:    $\delta$ , the sBeta hyper-parameter
3:    $\tau^-$ , the unimodal constraint
4:    $\tau^+$ , the constraint to avoid Dirac solutions
5: end global variables
6: function CONSTRAIN( $\alpha_k, \beta_k$ )
7:    $m_{sB} \leftarrow \frac{\alpha_k - 1 + \delta(\alpha_k - \beta_k)}{\alpha_k + \beta_k - 2}$   $\triangleright$  Estimate the mode
8:    $\lambda_k \leftarrow \alpha_k + \beta_k - 2$   $\triangleright$  Estimate the concentration
9:   for  $n \leftarrow 1 \dots D$  do
10:    if  $\lambda_{k,n} < \tau^-$  then
11:       $\lambda_{k,n} \leftarrow \tau^-$   $\triangleright$  Ensure strictly unimodal
solutions
12:    else if  $\lambda_{k,n} > \tau^+$  then
13:       $\lambda_{k,n} \leftarrow \tau^+$   $\triangleright$  Avoid Dirac solutions
14:    end if
15:   end for
16:    $\alpha_k \leftarrow 1 + \lambda_k \frac{m_{sB} + \delta}{1 + 2\delta}$   $\triangleright$  Update  $\alpha_k$  using (13)
17:    $\beta_k \leftarrow 1 + \lambda_k \frac{1 + \delta - m_{sB}}{1 + 2\delta}$   $\triangleright$  Update  $\beta_k$  using (13)
18:   return  $\alpha_k, \beta_k$ 
19: end function

```

4.3.3 Centroid initialization

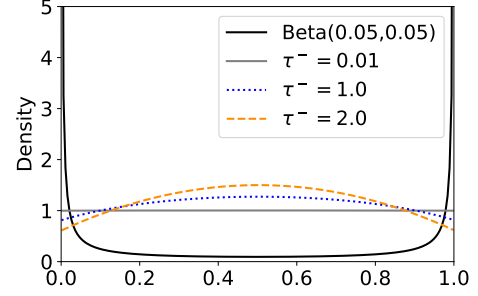
Clustering algorithms are known to be sensitive to their parameter initialization. They often converge to a local optimum. To reduce this limitation, the seeding initialization strategy k-means++, proposed in [30] and then thoroughly studied in [31], is broadly used for centroid initialization. However, in the context of the clustering of softmax predictions, we can assume that softmax predictions generated by deep learning models were optimized upstream to be sets of one-hot vectors⁷. Thus, we propose initializing the centroids as vertices of the target probability simplex domain. More specifically, we initialize all $\alpha_{k,n}$ and $\beta_{k,n}$ parameters such that they model exponential densities on $[0, 1]$ at the start. In other words, each initial mode is set as a vertex among all possible vertices on the probability simplex domain. Beyond improving K-SBETAS, this simple initialization strategy unanimously improves the scores of every tested clustering method⁸.

4.3.4 From cluster-label to class-label assignment

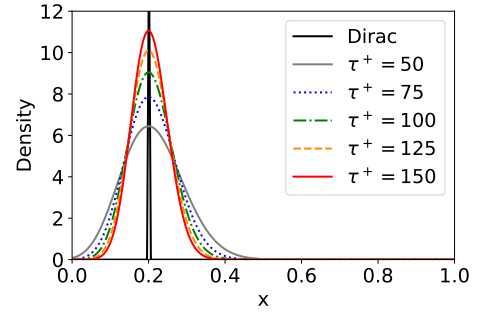
After clustering, we must align the obtained clusters with the target classes. One can align each cluster centroid with the closest one-hot vector by using the argmax function. However, in this case, a one-hot vector corresponding to a given class could be matched to several cluster centroids, thereby assigning them to the same class. To prevent this problem on closed-set challenges, i.e., with the prior knowledge $K = D$, we use the optimal transport Hungarian algorithm [32]. Specifically, we compute the Euclidean distances between all the centroids and one-hot vectors. Then, we apply the Hungarian algorithm to this matrix of distances to find the lowest-cost way, assigning a separate class to each cluster.

7. A one-hot vector both refers to a semantic class and to a vertex on the probability simplex.

8. Table 14 in Appendix empirically supports this statement.



(a) Avoid bimodal solutions



(b) Avoid Dirac solutions

Fig. 5: **Visualization of the introduced constraints.** Fig. (a) shows sBeta density estimation, constrained with the threshold τ^- , on a sample following a bimodal Beta distribution. Fig. (b) shows sBeta density estimation, constrained with the threshold τ^+ , on a sample following a Dirac distribution.

5 EXPERIMENTS

Throughout this section, we show different applications of the proposed method and compare it with the state-of-the-art clustering methods discussed in Sec. 3. We first validate our implementations on synthetic datasets and on real softmax predictions from unsupervised domain adaptation (UDA) source models (Sec. 5.1). Then, in Sec. 5.2, we demonstrate the usefulness of our simplex-clustering method in the context of transductive zero- and one-shot predictions using contrastive language-image pre-training (CLIP) [4] for the source model. Finally, we provide an application example for a dense prediction task: real-time UDA for road segmentation (Sec. 5.3). In each of these settings, our method is used as a plug-in on top of the output predictions from a black-box deep learning model. Along with the experiments and comparisons that follow, we also provide ablation studies, which highlight the effect of each component of the proposed framework.

Comparisons. We compare our method to several state-of-the-art clustering methods. Specifically, we include KL K-MEANS [10] [9] and HSC [12], which are specifically designed to deal with probability simplex vectors. We additionally compare our method to standard clustering methods: K-MEANS, GMM [33], K-MEDIANS [15], K-MEDOIDS [34] and K-MODES [16]. Both K-MEANS and KL K-MEANS use the mean as the cluster's parameter vector, with the former being based on the Euclidean distortion and the latter on the Kullback-Leibler one. Extensively studied in [15], K-MEDIANS uses

Algorithm 2 k-SBetas algorithm.

Input: Dataset of probability simplex points defined as $\mathcal{X} = \{\mathbf{x}_i\}_{i=1}^N \in \Delta^{D-1}$, with N the total number of points.
 Number of clusters K . The maximum number t_{end} of iterations.

Output: \mathbf{U} , the clustering hard label assignments

- 1: **global variables**
- 2: δ , the sBeta hyper-parameter
- 3: τ^- , the unimodal constraint
- 4: τ^+ , the constraint to avoid Dirac solutions
- 5: **end global variables**
- 6: $\mathbf{U} \leftarrow [0]_{N,K}$ \triangleright Arbitrary label initialization
- 7: $\boldsymbol{\pi} \leftarrow \{\frac{1}{K}\}_{k=1}^K$ \triangleright Initialize uniform class proportions
- 8: Initialize $\boldsymbol{\Theta}$ using *vertex init*. \triangleright Sec. 4.3.3.
- 9: $t \leftarrow 0$
- 10: **repeat**
- 11: **if** $t > 0$ **then**
- 12: **for** $k \leftarrow 1 \dots K$ **do** \triangleright Loop over clusters
- 13: Estimate $\boldsymbol{\alpha}_k, \boldsymbol{\beta}_k$ with MoM/MLE \triangleright Sec. 4.3.1.
- 14: $\boldsymbol{\alpha}_k, \boldsymbol{\beta}_k \leftarrow \text{CONSTRAIN}(\boldsymbol{\alpha}_k, \boldsymbol{\beta}_k)$ \triangleright Algorithm 1
- 15: **end for**
- 16: **end if**
- 17: **for** $i \leftarrow 1 \dots N$ **do** \triangleright hard label assignment
- 18: **for** $k \leftarrow 1 \dots K$ **do**
- 19: **if** $\arg \max_k \pi_k \cdot g_{\text{sBeta}}(\mathbf{x}_i; \boldsymbol{\alpha}_k, \boldsymbol{\beta}_k) = k$ **then**
- 20: $u_{i,k} \leftarrow 1$
- 21: **else**
- 22: $u_{i,k} \leftarrow 0$
- 23: **end if**
- 24: **end for**
- 25: **end for**
- 26: $\boldsymbol{\pi} \leftarrow \frac{\sum_{i=1}^N \mathbf{u}_i}{N}$ \triangleright Estimate class proportions
- 27: $t \leftarrow t + 1$
- 28: **until** convergence or $t = t_{end}$
- 29: **return** \mathbf{U}

the median as a cluster representative and the Manhattan distance. Clustering with K-MEDOIDS uses the Euclidean distance while estimating medoid representations of the clusters with the standard PAM algorithm [34]. Finally, K-MODES [16] uses a kernel-induced distortion and computes cluster modes via the Meanshift algorithm [35].

K-DIRS. We also implemented a simplex-clustering strategy, which estimates a multivariate density per cluster using the Dirichlet density function. We used the iterative parameter estimation proposed in [27]. This algorithm, which we refer to as K-DIRS, represents a baseline for the artificial datasets built from the Dirichlet distributions.

Proposed k-SBETAS. Our clustering algorithm uses f_{sBeta} as density function and the method of moments (MoM) detailed in Sec. 4.3.1 for parameter estimation. We empirically consolidate this choice in the ablation study in section 5.4. Note that K-BETAS corresponds to a non-scaled variant of K-SBETAS, i.e., when we set $\delta = 0$.

Hyper-parameters. Across all the experiments, we set the scaling hyper-parameter δ used in K-SBETAS to the same value 0.15. We set $\tau^- = 1$ and $\tau^+ = 165$ for parameter constraints. The maximum number of clustering iterations is set to 25 for all the clustering algorithms. For each method,

we use the parameter initialization detailed in Sec. 4.3.3. This technique is also applied to the methods based on the feature maps, for consistency and fairness: For each probability simplex vertex (i.e., one-hot vector), we select the feature-map point whose softmax prediction most closely aligns with this one-hot vector. We provide comparisons and justifications for our design choices in the ablation studies in Sec. 5.4.

Reproducibility. We used the implementation of the scikit-learn library for GMM⁹, and the implementation provided by the authors for HSC¹⁰. We have implemented all the other clustering algorithms¹¹.

Evaluation metrics. We use the standard *Normalized Mutual Information* (NMI) to evaluate the clustering task for each dataset. To evaluate the class-prediction scores, we use the classification *Accuracy* (Acc) for the balanced datasets or the *Intersection over Union* (IoU) measure for the imbalanced ones. The process of aligning the clusters with the class labels, which is necessary for computing the ACC and mIoU, is detailed in Sec. 4.3.4.

5.1 Unsupervised Domain Adaptation

5.1.1 Synthetic experiments

The purpose of the following synthetic experiments is to benchmark the different clustering methods on a simple, artificially generated task.

Simu dataset. We generate balanced mixtures composed of three Dirichlet distributions, defined on the 3-dimensional probability simplex, Δ^2 . The corresponding Dirichlet parameters are $\boldsymbol{\alpha}_1 = (1, 1, 5)$, $\boldsymbol{\alpha}_2 = (25, 5, 5)$, $\boldsymbol{\alpha}_3 = (5, 7, 5)$. Each component is made biased towards one different vertex of the simplex, thereby simulating the softmax predictions of a deep model for a certain class. Additionally, each component captures a different type of distribution¹²: $Dir(\boldsymbol{\alpha}_1)$ corresponds to an exponential distribution on Δ^2 , $Dir(\boldsymbol{\alpha}_2)$ to an off-centered distribution with small variance, and $Dir(\boldsymbol{\alpha}_3)$ to a more centered distribution, with a wider variance. All the components contribute equally to the final mixture. In total, 10^5 examples are sampled. We perform 5 random runs, each using new examples.

Results. The third column of Table 2 reports the NMI and Acc scores of different approaches on the Simu dataset. As expected, K-DIRS and K-BETAS yielded close scores as they both model the Beta marginal densities. K-SBETAS yields lower scores due to the scaling factor, $\delta > 0$. However, it behaves better than all the other clustering methods thanks to a proper statistical modeling of simplex data.

5.1.2 Clustering the softmax predictions of deep models

We now compare the different clustering approaches on real-world distributions, where data points correspond to

9. The GMM code is available at: https://github.com/scikit-learn/scikit-learn/blob/7e1ef6d09b/sklearn/mixture/_gaussian_mixture.py.

10. The HSC code is available at: <https://franknielsen.github.io/HSC/>.

11. The codes for KL K-MEANS, K-MEANS, K-MEDIANS, K-MEDOIDS, K-MODES, K-DIRS, K-BETAS and K-SBETAS are available at our repository: https://github.com/fchiaroni/Clustering_Softmax_Predictions

12. We provide the 2D visualizations of these simulated distributions in Appendix, Fig. 7.

TABLE 2: Comparative **probability simplex clustering** on **Simu**, **SVHN**→**MNIST** and **VISDA-C** datasets. The **FEATURE MAP** layer is the bottleneck layer on top of the convolutional layers. It outputs a feature vector of size 256 for each input image. The **LOGIT** points are obtained with the fully connected classifier on top of the bottleneck layer so that the logit point predicted for each input example is a vector of size K . The probability **SIMPLEX** points, which represent the predictions of a black-box model, are obtained with the standard softmax function on top of the **LOGIT** layer.

METHOD	LAYER USED	SIMU	SVHN→MNIST		VISDA-C
		(NMI)	(NMI)	(Acc)	(NMI)
K-MEANS	FEATURE MAP	-	67.3	74.3	30.0 22.7
K-MEANS	LOGIT	-	67.1	74.5	32.7 33.1
ARGMAX		60.1	58.6	69.8	36.5 53.1
K-MEANS		76.6	58.4	68.9	37.6 47.9
GMM		75.8	61.9	69.2	36.3 49.4
K-MEDIANS		76.8	58.6	68.8	35.9 40.0
K-MEDOIDS	SIMPLEX	60.8	58.9	71.3	36.5 46.8
K-MODES	(BLACK-BOX)	76.2	59.5	71.3	34.2 51.8
KL K-MEANS		76.2	63.3	75.5	39.8 51.2
HSC		9.3	59.2	68.9	28.7 18.1
K-DIRS		81.3	57.7	68.8	FAILS
K-BETAS		81.1	53.3	51.5	36.7 19.8
K-SBETAS		79.2	65.0	76.6	40.3 56.0

the softmax predictions of deep-learning models.

Setup. First, we employ the **SVHN**→**MNIST** challenge, where a source model is trained on SVHN [36] and applied to the MNIST [37] test set, which is composed of 10^4 images labelled with 10 different semantic classes. Additionally, we experiment with the more difficult **VISDA-C** challenge [38], which contains 55388 samples split into 12 different semantic classes. For both **SVHN**→**MNIST** and **VISDA-C**, we use the common network architectures and training procedures detailed in [39]. For these closed-set UDA experiments, we use the optimal-transport Hungarian algorithm to obtain cluster-to-class label assignment, as detailed in Sec. 4.3.4.

Results. Table 2 shows interesting comparative results for clustering real-world softmax predictions. In the **SVHN**→**MNIST** setting, simplex-tailored methods KL K-MEANS and K-SBETAS clearly stand out in terms of both the NMI and Accuracy. In particular, the proposed K-SBETAS achieves the best scores. On the **VISDA-C** challenge, however, KL K-MEANS yielded a performance below the baseline, similarly to the other standard clustering methods. K-DIRS failed to converge. In contrast, K-SBETAS outperforms the baseline by a margin, achieving the best scores.

Table 3 reports the running times of all the methods. When using MoM for parameter estimation, K-SBETAS has a running time close to or even lower than the standard GMM approach. Furthermore, a GPU-based implementation of K-SBETAS could be made even faster, which makes it appealing for large-scale datasets such as **VISDA-C**.

Feature maps vs. simplex predictions. Interestingly, Table 2 shows that k-means, when applied to the logit points, yields scores that are similar or even better than when applied to the feature maps. This suggests that the classifier head, which predicts the logit points, does not deteriorate the semantic

TABLE 3: **Computational time** comparison in seconds. All methods are executed on the same hardware: *CPU 11th Gen Intel(R) Core(TM) i7-11700K 3.60GHz*, and *GPU NVIDIA GeForce RTX 2070 SUPER*. MLE-1000 and MLE-500 refer to the MLE parameter estimation with a maximum of 1000 and 500 MLE iterations, respectively, while MoM refers to the method of moments.

METHOD	SVHN→MNIST	VISDA-C
	($N = 10000, K = 10$)	($N = 55388, K = 12$)
K-MEANS - FEATURE MAP	2.36	18.01
K-MEANS - LOGIT /SIMPLEX	0.06	1.27
GMM	0.43	10.59
K-MEDIANS	5.94	48.39
K-MEDOIDS	8.83	195.00
K-MODES	0.08	4.71
KL K-MEANS	0.27	2.79
HSC	8494.54	>ONE DAY
K-SBETAS (MLE-1000)	64.32	107.43
K-SBETAS (MLE-500)	34.22	58.68
K-SBETAS (MoM)	0.48	3.61
K-SBETAS (MoM, GPU-BASED)	0.13	0.49

information of the bottleneck layer. Table 3 shows that logit and simplex clustering are computationally less demanding than clustering the feature maps. This is due to the fact that the dimension of the simplex points is K , which is considerably smaller than the dimension of feature maps. In addition, Table 2 shows that the proposed simplex-clustering method substantially outperforms the K-MEANS feature-map clustering on the most difficult/realistic dataset, **VISDA-C**.

It is worth noting that the explored softmax-prediction datasets, **SVHN**→**MNIST** and **VISDA-C**, are challenging in this particular black-box setting. This enables interesting comparisons with model-agnostic clustering methods. For reproducibility and future improvements, we made these black-box softmax predictions publicly available: https://github.com/fchiaroni/Clustering_Softmax_Predictions.

5.2 Transductive zero-shot and one-shot learning

We now demonstrate the general applicability and effectiveness of our method in the practical and realistic few-shot problem, which involves only an unknown fraction of the original set of classes in a small, unlabeled query (test) set [40]. We tackle transductive zero- and one-shot inference using the foundational CLIP model [4] by clustering its zero-shot softmax predictions. CLIP is based on two deep encoders, one for image representation and the other for text inputs. Coupled with projections, this dual structure yields image and text embeddings within the same low-dimensional space. Trained on a large-scale dataset of text-image pairs, CLIP maximizes the cosine similarity between the embedding of an image and its corresponding text description, which makes it well-suited for zero-shot prediction. At inference time, the classification of a given image into one of K classes is given by the zero-shot softmax prediction of CLIP: $\sigma(z)_j = \frac{\exp(z_j)}{\sum_{i=1}^D \exp(z_i)}$, where logit z_j evaluates the cosine similarity between the image embedding and the representation of a text prompt describing the class, typically "a photo of a [name of class k]" [4]. In the one-shot setting, we cluster softmax predictions of the same form, except that, for each class, the text embedding

is replaced by the visual embedding of the labeled shot of the class, i.e., the single labeled image of the class.

Experimental Setup: We assessed our method using four distinct architectures of the CLIP visual encoder: ResNet-50, ResNet-101 [41], ViT-B/32, and ViT-B/16 [42]. Our experiments were performed across eight datasets: CIFAR-100 [43], Stanford-Cars [44], FGVC Aircraft [45], Caltech101 [46], Food101 [47], Flowers102 [48], Sun397-100 [49] and ImageNetv2-100 [50]. For Sun397-100 and ImageNetv2-100, we restrict the evaluation to the first 100 classes. For each dataset, we generated 100 query sets, each containing 64 unlabeled examples sampled from a random selection of 2 to 10 classes.

We compare our method with the inductive baseline, i.e., CLIP zero-shot prediction, and with transductive state-of-the-art few-shot learning methods, which leverage the statistics of the unlabeled query set, and operate on the feature maps: BD-CSPN [51], LAP-SHOT [52] and TIM [53]. Additional comparisons include K-MEANS, KL K-MEANS, and our K-SBETAS method, which we apply directly to the softmax predictions of CLIP. In the one-shot setting, the initialization prototype vector for each class is the CLIP-encoded image from the labeled support set. In the zero-shot setting, the initialization prototype vector for each class is the CLIP-encoded text prompt. Post-convergence, we directly employ the argmax function for cluster-to-class assignments. This function assigns each estimated cluster to the class whose one-hot vector is nearest to the cluster centroid.

Results. Tables 4 and 5 show the results for these One-shot and Zero-shot settings. A first key observation is the enhanced effectiveness of the probability-simplex methods over those based on the feature maps. On another note, one may observe that feature-map methods TIM and k-means show similar results in these settings. This observation is consistent with a previous work [54], which showed that, under certain mild conditions, along with common posterior models and parameter regularization, such models become equivalent. Overall, the proposed K-SBETAS method demonstrates a clear and consistent improvement over the inductive CLIP baseline and the other transductive few-shot methods across a variety of datasets and network encoders. This indicates its potential as a robust and versatile approach in enhancing the performance of foundation models, like CLIP, in practical applications with limited labeled data and unknown class distributions.

5.3 Real-Time UDA for road segmentation

We now consider a question that was, to the best of our knowledge, hitherto unaddressed in UDA segmentation: Can we adapt predictions from a black-box source model on a target set in real-time?

Setup. We address this question on the *road GTA5*→*road Cityscapes* challenge. A source model is trained on GTA5 [55] and applied on the Cityscapes validation set [56]. Following [57], we use Deeplab-V2 [58] as the semantic segmentation network. In our case, the model is exclusively trained for the binary task of road segmentation. The validation set contains

500 images with a 1024*2048 resolution. In order to simulate a real-time application, we treat each image independently, i.e. as a new clustering task, in which each pixel represents a point to cluster.

Towards Real-Time running time: Furthermore, to maximize the speed of execution, we downsample the model’s output probability map prior to fitting the clustering methods and then use the obtained densities to perform inference at the original resolution. Downsampling by a factor of 8 allows for an increase in the frame rate by almost two orders of magnitude, without incurring any loss in mIoU¹³. Specifically, K-SBETAS takes on average 0.0165 seconds for clustering on each 128*256 subset of pixels and 0.0056 seconds for predictions on original 1024*2048 images, which represents a processing frequency of 45 images per second. Hardware used: CPU 11th Gen Intel(R) Core(TM) i7-11700K 3.60GHz, and GPU NVIDIA GeForce RTX 2070 SUPER.

Results. Corresponding NMI and mean IoU scores are displayed on Table 6, and show K-SBETAS outperforming low computational demanding competitors K-MEANS and KL K-MEANS by a large margin, with an improvement of 14 mIoU points over the pixel-wise inductive baseline. Fig. 1 provides qualitative results, in which K-SBETAS yields a definite visual improvement over the baseline. In addition, and consistently with the previous results observed in Table 2 for the UDA classification challenge, Table 6 also shows that clustering the probability simplex points may be more effective than clustering the logits.

5.4 Ablation studies

Joint v.s. Factorised density. Our proposed method draws inspiration from a factorized Beta density, i.e. each component of the simplex vector is considered independent from each other. While such a simplifying assumption has significant analytical and computational benefits, it may also fail to capture the complexity of the target distribution. We explore this trade-off by comparing K-BETAS with K-DIRS, in which the full joint Beta density – corresponding to a Dirichlet density – is fitted at each iteration. Because there exists no closed-form solution to this problem, we resort to the approximate estimation procedure described in [27]. Results in Table 2 show that K-DIRS and K-BETAS produce similar scores on mixtures of Dirichlet distributions. In the meantime, K-DIRS outperforms K-BETAS on SVHN→MNIST but fails to converge on the more challenging VISDA-C challenge, making it ill-suited to real-world applications.

Effect of class imbalance. To investigate the problem of class imbalance, we generate heavily imbalanced datasets. First, we create an imbalanced version of our synthetic *Simu* dataset, which we refer to as *iSimu*. Specifically, we weighted the 3 components of the *Simu* mixture with six different combinations using the imbalanced class proportions {0.75, 0.2, 0.05}. Second, we consider a variant of VISDA-C, where class-proportions are sampled from a Dirichlet distribution with $\alpha = \mathbf{1}_K$. We refer to this variant as *iVISDA-Cs*. We perform 10 random re-runs.

13. See Table 13 in the Appendix for more details.

TABLE 4: 1-shot results. Query set size is 64. The proposed K-SBETAS further boosts the results of the existing CLIP model by clustering its soft predictions on the query set.

METHOD	LAYER USED	NETWORK	CIFAR-100		STANFORD-CARS		FGVC		CALTECH101		FOOD101		FLOWERS102		SUN397-100		IMAGENETV2-100	
			(NMI)	(Acc)	(NMI)	(Acc)	(NMI)	(Acc)	(NMI)	(Acc)	(NMI)	(Acc)	(NMI)	(Acc)	(NMI)	(Acc)	(NMI)	(Acc)
CLIP	FEATURE MAP	RN50	54.1	17.2	61.6	26.9	55.4	15.8	77.7	64.5	58.8	29.4	74.0	58.5	65.3	43.8	63.2	31.3
BD-CSPN	FEATURE MAP	RN50	54.1	13.8	60.3	19.7	56.1	13.7	70.0	51.1	57.4	22.7	70.5	46.8	60.4	32.6	61.8	25.2
LAP-SHOT	FEATURE MAP	RN50	54.1	13.9	60.3	19.7	56.0	13.7	70.2	51.3	57.4	22.8	70.5	46.8	60.5	32.8	61.8	25.2
TIM	FEATURE MAP	RN50	56.3	14.3	59.0	14.5	57.2	11.6	63.9	35.4	57.0	17.8	68.7	34.3	55.9	22.9	60.8	18.0
K-MEANS	FEATURE MAP	RN50	56.3	14.3	59.0	14.5	57.2	11.6	63.9	35.4	57.0	17.8	68.7	34.3	55.9	22.9	60.8	18.0
K-MEANS	SIMPLEX	RN50	52.1	17.5	65.6	29.3	55.5	16.0	79.6	63.9	60.2	31.4	80.1	65.3	69.9	45.7	65.6	31.5
KL K-MEANS	SIMPLEX	RN50	52.1	17.6	65.5	29.3	55.4	16.1	79.4	64.1	60.1	31.2	80.0	65.0	69.7	45.8	65.7	31.5
K-SBETAS	SIMPLEX	RN50	51.9	18.6	66.6	32.6	55.4	17.9	82.6	69.5	61.0	34.0	80.6	67.7	71.9	48.7	65.8	37.7
CLIP	FEATURE MAP	RN101	56.8	21.3	66.2	31.5	55.9	19.8	78.2	67.2	64.7	37.2	76.7	61.4	68.7	51.4	66.3	37.2
BD-CSPN	FEATURE MAP	RN101	56.6	17.4	63.5	23.6	55.8	16.3	69.3	53.1	63.4	30.2	71.9	48.6	62.8	39.1	65.1	31.1
LAP-SHOT	FEATURE MAP	RN101	56.6	17.4	63.5	23.6	55.8	16.3	69.4	53.2	63.4	30.3	71.9	48.7	62.8	39.3	65.1	31.2
TIM	FEATURE MAP	RN101	59.6	19.9	61.8	16.7	56.7	14.3	64.9	40.4	63.9	27.3	73.2	42.0	59.5	28.6	64.2	23.3
K-MEANS	FEATURE MAP	RN101	59.6	19.9	61.8	16.7	56.7	14.3	64.9	40.4	63.9	27.3	73.2	42.0	59.5	28.6	64.2	23.3
K-MEANS	SIMPLEX	RN101	57.1	21.8	72.6	35.0	58.5	20.1	79.9	66.5	67.3	40.6	84.9	67.6	72.3	52.7	71.0	41.5
KL K-MEANS	SIMPLEX	RN101	57.1	21.9	72.4	34.8	58.4	20.0	80.0	66.6	67.3	40.6	84.9	67.6	72.4	52.5	70.8	41.7
K-SBETAS	SIMPLEX	RN101	57.4	23.2	74.1	37.2	58.3	22.3	81.5	70.2	68.1	42.0	85.2	70.1	74.9	56.7	71.2	46.8
CLIP	FEATURE MAP	ViT-B/32	59.0	26.2	63.0	28.0	55.8	18.8	82.0	69.9	64.8	38.4	77.2	61.8	69.1	44.4	66.4	36.6
BD-CSPN	FEATURE MAP	ViT-B/32	58.5	21.7	60.8	21.5	55.9	15.2	73.1	57.7	62.4	30.6	71.7	49.9	63.8	36.4	65.0	30.6
LAP-SHOT	FEATURE MAP	ViT-B/32	58.6	21.8	60.8	21.5	55.9	15.3	73.4	57.8	62.5	30.7	71.7	49.9	64.0	36.6	65.0	30.6
TIM	FEATURE MAP	ViT-B/32	60.9	21.1	58.0	15.4	56.7	12.8	65.5	41.2	61.5	25.4	69.0	36.7	58.7	26.1	63.3	22.7
K-MEANS	FEATURE MAP	ViT-B/32	60.9	21.1	58.0	15.4	56.7	12.8	65.5	41.2	61.5	25.4	69.0	36.7	58.7	26.1	63.3	22.7
K-MEANS	SIMPLEX	ViT-B/32	60.2	26.4	68.0	29.9	58.1	19.3	84.4	69.7	66.1	39.8	85.3	67.2	72.7	46.0	70.9	38.2
KL K-MEANS	SIMPLEX	ViT-B/32	60.0	26.2	67.9	29.9	58.1	19.3	84.3	69.6	66.0	39.8	85.3	67.3	72.6	45.9	70.8	38.6
K-SBETAS	SIMPLEX	ViT-B/32	60.1	27.2	69.6	32.8	58.5	22.3	85.6	72.3	67.4	42.8	85.9	70.3	75.4	48.9	71.1	43.6
CLIP	FEATURE MAP	ViT-B/16	60.6	31.2	66.8	33.8	56.7	23.2	81.6	75.5	68.2	48.2	80.8	68.9	66.8	46.3	69.2	43.0
BD-CSPN	FEATURE MAP	ViT-B/16	59.9	26.2	64.7	26.6	56.0	18.9	71.3	60.2	65.2	38.5	76.7	57.1	62.7	35.5	66.6	35.1
LAP-SHOT	FEATURE MAP	ViT-B/16	60.0	26.3	64.8	26.7	56.0	18.9	71.5	60.2	65.2	38.7	76.8	57.1	62.7	35.4	66.8	35.2
TIM	FEATURE MAP	ViT-B/16	63.3	26.0	61.4	18.3	56.9	15.0	63.8	44.0	62.7	28.1	75.2	45.7	58.0	26.4	63.8	25.2
K-MEANS	FEATURE MAP	ViT-B/16	63.3	26.0	61.4	18.3	56.9	15.0	63.8	44.0	62.7	28.1	75.2	45.7	58.0	26.4	63.8	25.2
K-MEANS	SIMPLEX	ViT-B/16	61.3	30.2	71.3	34.3	61.6	23.7	82.7	73.3	70.3	48.9	87.9	74.5	70.4	47.4	76.8	46.7
KL K-MEANS	SIMPLEX	ViT-B/16	61.1	30.2	71.1	34.4	61.5	23.8	82.5	73.2	70.2	48.6	87.8	74.5	70.3	47.3	76.8	47.1
K-SBETAS	SIMPLEX	ViT-B/16	61.2	32.3	73.3	38.3	62.1	25.2	85.9	79.1	72.4	54.7	88.6	78.9	72.7	50.2	77.1	50.5

Table 7 compares the clustering models on these two datasets. Displayed NMI scores for *iSimus* correspond to the average NMI scores obtained across the six different mixture proportions. NMI and IoU scores displayed for iVISDA-Cs correspond to the average scores obtained across ten different highly imbalanced subset variants of VISDA-C. K-SBETAS (BIASED) refers to the proposed approach without the marginal probability term π_k in eq. 14. These comparative results clearly highlight the benefit of the proposed K-SBETAS formulation. Note that our unbiased formulation could theoretically apply to metric-based approaches but was systematically found to produce degenerated solutions in which all examples are assigned to a unique cluster.

Parameter estimation. Concerning the parameter estimation for K-SBETAS, we can observe in Table 3 and Table 8 that using the method of moments (MoM) is more beneficial than the iterative MLE in practice, both in terms of computational cost and prediction performances.

Effect of the unimodal constraint. Table 8 empirically confirms that constraining a density-based clustering model to only consider mixtures of unimodal distributions is appropriate with softmax predictions from pre-trained source models. Yet, we can observe that disabling this constraint has no impact on K-SBETAS results. The following paragraph explains such observations by the presence of δ .

Effect of δ . As a matter of fact, Table 8 results suggest that δ interest is finally twofold in our experiments: It enables a more flexible clustering. Meanwhile, it also prevents estimating bimodal density functions. The latter point

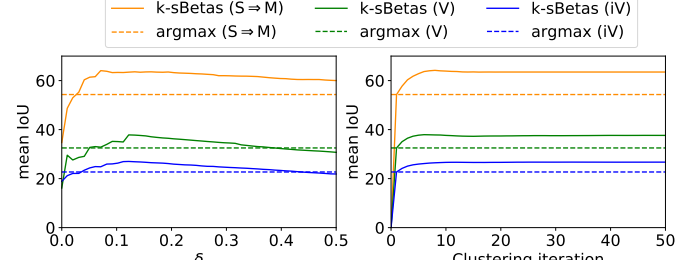


Fig. 6: K-SBETAS mean IoU scores depending on δ and on the clustering iteration. We respectively set 25 clustering iterations on the left figure and $\delta = 0.15$ on the right one. S \rightarrow M, V, and iV respectively refer to SVHN \rightarrow MNIST, VISDA-C, and iVISDA-Cs datasets.

can be explained as follows. Bimodal distributions have a higher variance than uniform or unimodal distributions because they partition the major portion of the density at the vicinity of two opposite interval boundaries simultaneously. Thus, when δ is sufficiently large (e.g. with $\delta = 0.15$ in these experiments), the scaled variance of the projection of \mathbf{x}_i coordinates into the interval $[\frac{\delta}{1+2\delta}, \frac{1+\delta}{1+2\delta}]$ becomes sufficiently small to inhibit the modeling of bimodal distributions. Complementary, Fig. 6 shows that setting $\delta = 0.15$ provides consistent outperforming results on different datasets, and it allows fast convergence in terms of clustering iterations. Thus, we set $\delta = 0.15$ along all the other presented experiments.

Pre-clustering: Centroid initialization. Parameter initialization plays a crucial role in unsupervised clustering.

TABLE 5: **0-shot results. Query set size is 64.** The proposed K-SBETAS further boosts the results of the existing Zero-Shot CLIP model by clustering its soft predictions on the query set.

METHOD	LAYER USED	NETWORK	CIFAR-100		STANFORD-CARS		FGVC		CALTECH101		FOOD101		FLOWERS102		SUN397-100		IMAGENETV2-100	
			(NMI)	(Acc)	(NMI)	(Acc)	(NMI)	(Acc)	(NMI)	(Acc)	(NMI)	(Acc)	(NMI)	(Acc)	(NMI)	(Acc)	(NMI)	(Acc)
CLIP	FEATURE MAP	RN50	61.0	38.9	74.3	55.3	57.3	17.6	87.3	81.3	77.8	71.0	81.8	63.2	76.4	71.9	74.1	60.8
BD-CSPN	FEATURE MAP	RN50	58.7	23.4	68.6	25.8	56.1	6.5	77.2	47.4	69.8	37.8	75.0	29.5	66.6	41.2	68.1	31.8
LAP-SHOT	FEATURE MAP	RN50	56.3	19.6	69.6	25.3	55.1	5.5	77.4	46.3	66.3	29.8	61.5	12.7	66.9	41.5	66.2	27.1
TIM	FEATURE MAP	RN50	60.5	28.3	61.9	19.6	57.9	11.7	66.4	42.6	66.2	37.9	72.0	37.1	57.1	25.7	64.0	29.4
K-MEANS	FEATURE MAP	RN50	60.5	28.3	61.9	19.6	57.9	11.7	66.4	42.6	66.2	37.9	72.0	37.1	57.1	25.7	64.0	29.4
K-MEANS	SIMPLEX	RN50	63.4	40.4	80.2	59.0	60.1	18.8	90.7	84.6	81.8	79.2	90.6	69.0	81.3	74.8	78.2	69.2
KL K-MEANS	SIMPLEX	RN50	63.4	40.5	80.2	59.0	60.0	18.9	90.8	84.6	81.8	79.2	90.5	68.8	81.4	75.1	78.2	69.3
K-SBETAS	SIMPLEX	RN50	64.5	43.2	83.6	64.2	61.1	20.4	91.7	85.4	83.3	81.6	91.0	69.1	84.8	80.7	79.3	72.2
CLIP	FEATURE MAP	RN101	59.5	42.7	77.9	62.8	57.4	18.1	86.1	83.3	80.0	74.5	80.1	61.0	78.4	71.5	77.3	67.7
BD-CSPN	FEATURE MAP	RN101	56.9	24.4	70.7	34.0	57.5	7.7	77.3	45.9	70.6	38.5	78.1	28.9	69.8	44.4	71.0	34.1
LAP-SHOT	FEATURE MAP	RN101	53.7	22.6	72.7	35.3	56.3	7.1	78.7	45.0	70.4	37.4	78.1	28.0	70.6	45.3	72.0	35.1
TIM	FEATURE MAP	RN101	63.3	36.8	63.6	25.4	59.4	14.1	69.4	51.9	70.2	49.4	74.5	38.8	64.1	36.5	67.7	38.6
K-MEANS	FEATURE MAP	RN101	63.3	36.8	63.6	25.4	59.4	14.1	69.4	51.9	70.2	49.4	74.5	38.8	64.1	36.5	67.7	38.6
K-MEANS	SIMPLEX	RN101	65.2	46.3	83.2	66.0	62.5	20.0	89.6	85.2	84.1	82.1	90.0	66.3	83.0	74.5	83.3	77.0
KL K-MEANS	SIMPLEX	RN101	65.2	46.4	83.2	66.1	62.5	20.0	89.6	85.1	84.0	82.2	89.9	66.3	82.8	74.3	83.3	77.0
K-SBETAS	SIMPLEX	RN101	64.2	47.6	86.9	70.5	63.9	21.7	91.3	86.8	84.9	83.3	90.6	66.7	85.0	78.0	84.9	79.6
CLIP	FEATURE MAP	ViT-B/32	70.4	58.9	75.8	59.1	57.8	17.6	89.8	85.4	78.9	76.2	81.7	62.0	79.0	72.9	77.1	63.6
BD-CSPN	FEATURE MAP	ViT-B/32	65.7	36.8	68.5	30.2	58.0	10.5	78.9	51.0	69.1	46.5	77.9	28.3	68.9	46.0	70.7	36.3
LAP-SHOT	FEATURE MAP	ViT-B/32	64.9	35.2	69.1	29.5	57.7	9.9	79.6	50.2	69.0	43.4	75.2	21.6	69.5	46.3	69.7	32.3
TIM	FEATURE MAP	ViT-B/32	65.0	38.9	62.2	22.0	58.1	12.7	66.8	44.5	65.5	42.1	73.6	38.7	59.1	30.4	66.2	33.7
K-MEANS	FEATURE MAP	ViT-B/32	65.0	38.9	62.2	22.0	58.1	12.7	66.8	44.5	65.5	42.1	73.6	38.7	59.1	30.4	66.2	33.7
K-MEANS	SIMPLEX	ViT-B/32	74.7	65.3	81.1	61.2	60.9	17.8	92.0	88.0	84.4	83.6	91.1	66.4	83.3	75.9	83.0	73.0
KL K-MEANS	SIMPLEX	ViT-B/32	74.8	65.4	81.1	61.3	60.8	17.4	91.9	88.0	84.4	83.7	91.1	66.3	83.4	76.2	83.0	73.0
K-SBETAS	SIMPLEX	ViT-B/32	75.9	67.7	85.2	68.2	61.9	18.9	94.5	88.9	86.1	86.0	91.2	67.1	85.7	79.5	83.5	74.5
CLIP	FEATURE MAP	ViT-B/16	71.0	63.8	79.1	63.7	61.1	26.0	91.0	86.2	85.1	82.9	83.1	66.4	79.7	75.6	79.6	70.5
BD-CSPN	FEATURE MAP	ViT-B/16	66.3	43.6	71.5	34.5	61.6	13.9	80.7	62.3	74.8	56.2	80.7	34.6	69.5	50.8	71.9	38.2
LAP-SHOT	FEATURE MAP	ViT-B/16	65.7	40.7	72.9	33.6	61.6	12.8	81.4	61.1	74.9	54.2	81.5	31.3	70.0	51.8	72.7	36.1
TIM	FEATURE MAP	ViT-B/16	65.8	44.4	64.2	25.0	60.6	15.8	70.4	49.5	70.1	48.9	75.1	43.8	60.0	31.3	66.3	38.8
K-MEANS	FEATURE MAP	ViT-B/16	65.8	44.4	64.2	25.0	60.6	15.8	70.4	49.5	70.1	48.9	75.1	43.8	60.0	31.3	66.3	38.8
K-MEANS	SIMPLEX	ViT-B/16	75.6	68.0	84.1	65.7	66.3	26.4	93.0	87.8	89.9	88.9	91.3	70.1	83.7	77.4	85.6	77.2
KL K-MEANS	SIMPLEX	ViT-B/16	75.6	68.1	84.1	65.8	66.3	26.6	92.9	87.8	89.9	88.9	91.3	70.1	83.7	77.4	85.8	77.2
K-SBETAS	SIMPLEX	ViT-B/16	77.3	71.6	87.3	70.4	68.2	28.7	93.9	88.1	90.8	90.3	91.2	70.6	86.9	82.8	86.5	79.7

TABLE 6: **Real-Time UDA** for road segmentation per image on the challenge GTA5→Cityscapes, by using probability simplex clustering.

APPROACH	GTA5→CITYSCAPES	
	(NMI)	(MIoU)
K-MEANS - LOGITS	21.4	39.4
ARGMAX	19.7	49.2
K-MEANS	23.6	52.4
KL K-MEANS	24.9	52.2
K-SBETAS	35.8	65.7

TABLE 7: Comparative probability simplex clustering on highly imbalanced iSimus and iVISDA-Cs datasets.

APPROACH	iSIMUS		IVISDA-CS	
	(NMI)	(MIoU)	(NMI)	(MIoU)
ARGMAX	55.5	31.6	22.7	
K-MEANS	62.3	32.8	24.2	
GMM	64.5	34.4	21.1	
K-MEDIANs	60.4	33.1	22.4	
K-MEDOIDS	62.6	32.1	22.5	
K-MODES	55.1	32.0	22.8	
KL K-MEANS	59.9	35.2	24.9	
HSC	17.7	28.9	16.3	
K-SBETAS (BIASED)	55.3	35.4	25.6	
K-SBETAS	72.4	36.4	27.1	

In Table 9, we compare the widely-used k-means++ initialization, designed for generic clustering, with our simplex-tailored vertex initialization. Regardless of the assignment method used, our initialization demonstrates up

TABLE 8: Accuracy depending on the unimodal constraint. The constraint is enabled in ✓ columns. k-Dirs parameter estimation [27] fails to converge on VISDA-C.

UNIMODAL CONSTRAINT	SVHN→MNIST		VISDA-C	
	✗	✓	✗	✓
K-DIRS	65.3	68.8	FAILS	FAILS
K-BETAS	19.5	51.5	11.9	19.8
K-SBETAS (MLE-500)	76.2	76.2	55.0	55.0
K-SBETAS	76.6	76.6	56.0	56.0

to a 7% improvement in accuracy over k-means++¹⁴.

Post-clustering: Cluster to class assignment. We also show on Table 9 the interest of the Hungarian algorithm, referred to as Hung, for aligning cluster-labels with class-labels. Compared to the argmax assignment for centroids in the context of such closed-set challenges, we recall that Hung aims to ensure that each cluster is assigned to a separate class. We can observe that the proposed Hung strategy is particularly interesting when using the vertex init. This suggests that optimal transport assignment is naturally relevant in situations where each cluster is likely to represent a separate class.

In order to provide a fair comparison with the state-of-the-art, we jointly applied these *pre-* and *post-*clustering strategies on every compared approach.

14. Table 14 in the Appendix further extends this comparison to other clustering approaches, showing similar benefits across every tested approach.

TABLE 9: K-SBETAS prediction performances depending on the parameter initialization and cluster to class assignment. We compare k-means++ with the proposed *vertex init*, and also the centroid assignment argmax with the proposed optimal transport strategy (Hung).

APPROACH	INIT	ASSIGNMENT	SVHN→MNIST	VISDA-C
			(ACC)	(ACC)
K-SBETAS	K-MEAN++	ARGMAX	69.0 ± 6.1	50.0 ± 5.0
	K-MEANS++	HUNG	69.8 ± 8.1	47.2 ± 5.2
VERTEX INIT	VERTEX INIT	ARGMAX	73.5 ± 0.0	53.8 ± 0.0
	VERTEX INIT	HUNG	76.6 ± 0.0	56.0 ± 0.0

6 DISCUSSION

This section discusses the potential limitations and extensions of the proposed approach.

Maximum performance may be upper-bounded. We have shown that clustering softmax predictions with the proposed approach can efficiently improve source model prediction performances at a reasonable computational footprint. However, it is worth noting that we could not reach the prediction performances of the recent state-of-the-art self-training [3], which exploits and updates the model parameters end-to-end through an iterative process. This is because, as for every clustering algorithm, the maximum performance of the proposed approach is upper-bounded by the quality of the output probability simplex domain representation, over which we have no control.

Spatial analysis could be complementary. The clustering model does not consider global or local spatial information. That would be worthwhile in challenges such as semantic pixel-wise segmentation to complement it with spatial post-processing techniques [59].

Clustering softmax predictions for self-training. Throughout this article, we have motivated the use of simplex clustering for efficient prediction adjustment of black-box source models. Nevertheless, simplex clustering could also play the role of pseudo-labeling along self-training strategies. This could be a simple and light generic alternative to feature map clustering [11], which would not imply cumbersome manipulation of high-dimensional and hidden feature maps.

If the number of classes is large. In some contexts, the number of classes K may be potentially large. For example, K may correspond to millions of words in neural language modeling. It would be then interesting to envision strategies that reorganize the softmax layer for more efficient calculation [60]. In addition, distortion-based and probabilistic clustering methods usually require a sufficient number of points per class to produce consistent partitioning. Thus, if K is too large with respect to the target set size, then the clustering could produce degenerate solutions. It would be interesting to explore hierarchical clustering strategies [61], [62] on the probability simplex domain, as these models can deal with a small amount of data points per class.

Low-powered devices. Systems such as mobile robots and embedded systems may not have the resources to perform costly neural network parameter updates on the application time. The presented framework can be viewed as an efficient plug-in solution for prediction adjustment in the wild when using such low-powered devices.

7 CONCLUSION

In this paper, we have tackled the simplex clustering of softmax predictions from black-box deep networks. We found that existing distortion-based objectives of the state-of-the-art do not adequately approximate real-world simplex distributions, which can, for example, be highly peaked near the simplex vertices. Thus, we have introduced a novel probabilistic clustering objective that integrates a generalization of the Beta density, which we coin sBeta. This scaled variant of Beta is relatively more permissive; meanwhile, we constrain it to fit only strictly unimodal distributions and to avoid degenerate solutions. In order to optimize our clustering objective, we proceed with a block-coordinate descent approach, which alternates optimization w.r.t assignment variables and parameter estimation of cluster distributions, s.t. the introduced parameter constraints. The resulting clustering model, which we refer to as K-SBETAS, is both highly competitive and efficient on the proposed simulated and real-world softmax-prediction datasets, including class-imbalance scenarios, along which we performed our comparisons. Additionally, we emphasized the utility of probability simplex clustering through several practical applications: zero-shot and one-shot image classification, and real-time adjustment for road segmentation on full-size images.

Our future perspectives include extending the insights of probability simplex clustering to other challenges, such as pseudo-labeling for self-training procedures and other applications that require rapid correction of source models. Moreover, it may be interesting to complement the clustering with spatial and temporal information depending on the target data properties.

Overall, we hope that the presented simplex clustering framework and softmax-prediction benchmarks will encourage the community to give more attention to such facilitating, low-computational demanding, model-agnostic, plug-in solutions.

ACKNOWLEDGMENTS

This research was supported by computational resources provided by Compute Canada.

REFERENCES

- [1] D. Wang, E. Shelhamer, S. Liu, B. Olshausen, and T. Darrell, “Tent: Fully test-time adaptation by entropy minimization,” in *International Conference on Learning Representations*, 2021.
- [2] M. Wang and W. Deng, “Deep visual domain adaptation: A survey,” *Neurocomputing*, vol. 312, pp. 135–153, 2018.
- [3] J. Liang, D. Hu, Y. Wang, R. He, and J. Feng, “Source data-absent unsupervised domain adaptation through hypothesis transfer and labeling transfer,” *IEEE Transactions on Pattern Analysis and Machine Intelligence*, 2021.
- [4] A. Radford, J. W. Kim, C. Hallacy, A. Ramesh, G. Goh, S. Agarwal, G. Sastry, A. Askell, P. Mishkin, J. Clark *et al.*, “Learning transferable visual models from natural language supervision,” in *International Conference on Machine Learning (ICML)*, 2021, pp. 8748–8763.

[5] H. Xia, H. Zhao, and Z. Ding, "Adaptive adversarial network for source-free domain adaptation," in *Proceedings of the IEEE/CVF International Conference on Computer Vision (ICCV)*, October 2021, pp. 9010–9019.

[6] P. Colombo, V. Pellegrain, M. Boudiaf, V. Storchan, M. Tami, I. B. Ayed, C. Hudelot, and P. Piantanida, "Transductive learning for textual few-shot classification in api-based embedding models," in *Empirical Methods in Natural Language Processing (EMNLP)*, 2023.

[7] F. Pereira, N. Tishby, and L. Lee, "Distributional clustering of english words," *arXiv preprint cmp-lg/9408011*, 1994.

[8] A. Banerjee, S. Merugu, I. S. Dhillon, J. Ghosh, and J. Lafferty, "Clustering with bregman divergences." *Journal of machine learning research*, vol. 6, no. 10, 2005.

[9] J. Wu, H. Xiong, and J. Chen, "Sail: Summation-based incremental learning for information-theoretic clustering," in *Proceedings of the 14th ACM SIGKDD international conference on knowledge discovery and data mining*, 2008, pp. 740–748.

[10] K. Chaudhuri and A. McGregor, "Finding metric structure in information theoretic clustering," in *COLT*, vol. 8. Citeseer, 2008, p. 10.

[11] M. Caron, P. Bojanowski, A. Joulin, and M. Douze, "Deep clustering for unsupervised learning of visual features," in *Proceedings of the European Conference on Computer Vision (ECCV)*, 2018, pp. 132–149.

[12] F. Nielsen and K. Sun, "Clustering in hilbert's projective geometry: The case studies of the probability simplex and the ellipotope of correlation matrices," in *Geometric Structures of Information*. Springer, 2019, pp. 297–331.

[13] R. O. Duda, P. E. Hart, and D. G. Stork, *Pattern Classification*, 2nd ed. John Wiley and Sons, 2000.

[14] D. Aloise, A. Deshpande, P. Hansen, and P. Popat, "Np-hardness of euclidean sum-of-squares clustering," *Machine Learning*, vol. 75, no. 2, pp. 245–248, 2009.

[15] P. S. Bradley, O. L. Mangasarian, and W. N. Street, "Clustering via concave minimization," *Advances in neural information processing systems*, pp. 368–374, 1997.

[16] M. A. Carreira-Perpiñán and W. Wang, "The k-modes algorithm for clustering," *arXiv preprint arXiv:1304.6478*, 2013.

[17] I. M. Ziko, E. Granger, and I. B. Ayed, "Scalable laplacian k-modes," in *Neural Information Processing Systems (NeurIPS)*, 2018, pp. 10 062–10 072.

[18] A. Krause, P. Perona, and R. Gomes, "Discriminative clustering by regularized information maximization," *Advances in neural information processing systems*, vol. 23, 2010.

[19] D. J. Rezende, S. Mohamed, and D. Wierstra, "Stochastic backpropagation and approximate inference in deep generative models," in *International conference on machine learning*. PMLR, 2014, pp. 1278–1286.

[20] W. Hu, T. Miyato, S. Tokui, E. Matsumoto, and M. Sugiyama, "Learning discrete representations via information maximizing self-augmented training," in *International conference on machine learning*. PMLR, 2017, pp. 1558–1567.

[21] S. Claić, M. Yurochkin, S. Ghosh, and J. Solomon, "Model fusion with kullback-leibler divergence," in *International Conference on Machine Learning*. PMLR, 2020, pp. 2038–2047.

[22] T. F. Gonzalez, "Clustering to minimize the maximum intercluster distance," *Theoretical computer science*, vol. 38, pp. 293–306, 1985.

[23] R. Panigrahy and S. Vishwanathan, "Ano ($\log^* n$) approximation algorithm for the asymmetric p-center problem," *Journal of Algorithms*, vol. 27, no. 2, pp. 259–268, 1998.

[24] Y. Boykov, H. Isack, C. Olsson, and I. Ben Ayed, "Volumetric bias in segmentation and reconstruction: Secrets and solutions," in *IEEE International Conference on Computer Vision (ICCV)*, 2015, pp. 1769–1777.

[25] M. Tang, D. Marin, I. B. Ayed, and Y. Boykov, "Kernel cuts: Kernel and spectral clustering meet regularization," *International Journal of Computer Vision*, vol. 127, no. 5, pp. 477–511, 2019.

[26] M. Kearns, Y. Mansour, and A. Y. Ng, "An information-theoretic analysis of hard and soft assignment methods for clustering," in *Learning in graphical models*. Springer, 1998, pp. 495–520.

[27] T. Minka, "Estimating a dirichlet distribution," 2000.

[28] M. J. Wainwright, M. I. Jordan *et al.*, "Graphical models, exponential families, and variational inference," *Foundations and Trends® in Machine Learning*, vol. 1, no. 1–2, pp. 1–305, 2008.

[29] J. Kruschke, *Doing Bayesian data analysis: A tutorial with R, JAGS, and Stan*. Academic Press, 2014.

[30] D. Arthur and S. Vassilvitskii, "k-means++: The advantages of careful seeding," Stanford, Tech. Rep., 2006.

[31] O. Bachem, M. Lucic, S. H. Hassani, and A. Krause, "Approximate k-means++ in sublinear time," in *Thirtieth AAAI conference on artificial intelligence*, 2016.

[32] H. W. Kuhn, "The hungarian method for the assignment problem," *Naval research logistics quarterly*, vol. 2, no. 1–2, pp. 83–97, 1955.

[33] C. Biernacki, G. Celeux, and G. Govaert, "Assessing a mixture model for clustering with the integrated completed likelihood," *IEEE transactions on pattern analysis and machine intelligence*, vol. 22, no. 7, pp. 719–725, 2000.

[34] L. Kaufman and P. J. Rousseeuw, "Partitioning around medoids (program pam)," *Finding groups in data: an introduction to cluster analysis*, vol. 344, pp. 68–125, 1990.

[35] Y. Cheng, "Mean shift, mode seeking, and clustering," *IEEE transactions on pattern analysis and machine intelligence*, vol. 17, no. 8, pp. 790–799, 1995.

[36] Y. Netzer, T. Wang, A. Coates, A. Bissacco, B. Wu, and A. Y. Ng, "Reading digits in natural images with unsupervised feature learning," in *NIPS Workshop*, 2011.

[37] Y. LeCun, L. Bottou, Y. Bengio, and P. Haffner, "Gradient-based learning applied to document recognition," *Proceedings of the IEEE*, vol. 86, no. 11, pp. 2278–2324, 1998.

[38] X. Peng, B. Usman, N. Kaushik, D. Wang, J. Hoffman, and K. Saenko, "Visda: A synthetic-to-real benchmark for visual domain adaptation," in *Proceedings of the IEEE Conference on Computer Vision and Pattern Recognition Workshops*, 2018, pp. 2021–2026.

[39] J. Liang, D. Hu, and J. Feng, "Do we really need to access the source data? source hypothesis transfer for unsupervised domain adaptation," in *International Conference on Machine Learning*. PMLR, 2020, pp. 6028–6039.

[40] S. Martin, M. Boudiaf, É. Chouzenoux, J. Pesquet, and I. B. Ayed, "Towards practical few-shot query sets: Transductive minimum description length inference," in *Neural Information Processing Systems (NeurIPS)*, 2022.

[41] K. He, X. Zhang, S. Ren, and J. Sun, "Deep residual learning for image recognition," in *Proceedings of the IEEE conference on computer vision and pattern recognition*, 2016, pp. 770–778.

[42] A. Dosovitskiy, L. Beyer, A. Kolesnikov, D. Weissenborn, X. Zhai, T. Unterthiner, M. Dehghani, M. Minderer, G. Heigold, S. Gelly, J. Uszkoreit, and N. Houlsby, "An image is worth 16x16 words: Transformers for image recognition at scale," in *International Conference on Learning Representations*, 2021. [Online]. Available: <https://openreview.net/forum?id=YicbFdNTTy>

[43] A. Krizhevsky, G. Hinton *et al.*, "Learning multiple layers of features from tiny images," 2009.

[44] J. Krause, M. Stark, J. Deng, and L. Fei-Fei, "3d object representations for fine-grained categorization," in *Proceedings of the IEEE international conference on computer vision workshops*, 2013, pp. 554–561.

[45] S. Maji, E. Rahtu, J. Kannala, M. Blaschko, and A. Vedaldi, "Fine-grained visual classification of aircraft," *arXiv preprint arXiv:1306.5151*, 2013.

[46] L. Fei-Fei, R. Fergus, and P. Perona, "Learning generative visual models from few training examples: An incremental bayesian approach tested on 101 object categories," in *Conference on Computer Vision and Pattern Recognition Workshop*, 2004, pp. 178–178.

[47] L. Bossard, M. Guillaumin, and L. Van Gool, "Food-101-mining discriminative components with random forests," in *Computer Vision–ECCV 2014: 13th European Conference, Zurich, Switzerland, September 6–12, 2014, Proceedings, Part VI 13*. Springer, 2014, pp. 446–461.

[48] M.-E. Nilsback and A. Zisserman, "Automated flower classification over a large number of classes," in *2008 Sixth Indian conference on computer vision, graphics & image processing*. IEEE, 2008, pp. 722–729.

[49] J. Xiao, J. Hays, K. A. Ehinger, A. Oliva, and A. Torralba, "Sun database: Large-scale scene recognition from abbey to zoo," in *2010 IEEE computer society conference on computer vision and pattern recognition*. IEEE, 2010, pp. 3485–3492.

[50] B. Recht, R. Roelofs, L. Schmidt, and V. Shankar, "Do imagenet classifiers generalize to imagenet?" in *International conference on machine learning*. PMLR, 2019, pp. 5389–5400.

[51] J. Liu, L. Song, and Y. Qin, "Prototype rectification for few-shot learning," in *Computer Vision–ECCV 2020: 16th European Conference, Glasgow, UK, August 23–28, 2020, Proceedings, Part I 16*. Springer, 2020, pp. 741–756.

- [52] I. Ziko, J. Dolz, E. Granger, and I. B. Ayed, "Laplacian regularized few-shot learning," in *International conference on machine learning*. PMLR, 2020, pp. 11 660–11 670.
- [53] M. Boudiaf, I. Ziko, J. Rony, J. Dolz, P. Piantanida, and I. Ben Ayed, "Information maximization for few-shot learning," *Advances in Neural Information Processing Systems*, vol. 33, pp. 2445–2457, 2020.
- [54] M. Jabi, M. Pedersoli, A. Mitiche, and I. B. Ayed, "Deep clustering: On the link between discriminative models and k-means," *IEEE transactions on pattern analysis and machine intelligence*, vol. 43, no. 6, pp. 1887–1896, 2019, publisher: IEEE.
- [55] S. R. Richter, V. Vineet, S. Roth, and V. Koltun, "Playing for data: Ground truth from computer games," in *European conference on computer vision*. Springer, 2016, pp. 102–118.
- [56] M. Cordts, M. Omran, S. Ramos, T. Rehfeld, M. Enzweiler, R. Benenson, U. Franke, S. Roth, and B. Schiele, "The cityscapes dataset for semantic urban scene understanding," in *Proceedings of the IEEE Conference on Computer Vision and Pattern Recognition (CVPR)*, June 2016.
- [57] T.-H. Vu, H. Jain, M. Bucher, M. Cord, and P. Pérez, "Advent: Adversarial entropy minimization for domain adaptation in semantic segmentation," in *Proceedings of the IEEE/CVF Conference on Computer Vision and Pattern Recognition*, 2019, pp. 2517–2526.
- [58] L.-C. Chen, G. Papandreou, I. Kokkinos, K. Murphy, and A. L. Yuille, "Deeplab: Semantic image segmentation with deep convolutional nets, atrous convolution, and fully connected crfs," *IEEE transactions on pattern analysis and machine intelligence*, vol. 40, no. 4, pp. 834–848, 2017.
- [59] V. Badrinarayanan, A. Kendall, and R. Cipolla, "Segnet: A deep convolutional encoder-decoder architecture for image segmentation," *IEEE transactions on pattern analysis and machine intelligence*, vol. 39, no. 12, pp. 2481–2495, 2017.
- [60] W. Chen, D. Grangier, and M. Auli, "Strategies for training large vocabulary neural language models," in *Proceedings of the 54th Annual Meeting of the Association for Computational Linguistics (Volume 1: Long Papers)*. Berlin, Germany: Association for Computational Linguistics, Aug. 2016, pp. 1975–1985.
- [61] F. Murtagh and P. Contreras, "Algorithms for hierarchical clustering: an overview," *Wiley Interdisciplinary Reviews: Data Mining and Knowledge Discovery*, vol. 2, no. 1, pp. 86–97, 2012.
- [62] G. Ahalya and H. M. Pandey, "Data clustering approaches survey and analysis," in *2015 International Conference on Futuristic Trends on Computational Analysis and Knowledge Management (ABLAZE)*. IEEE, 2015, pp. 532–537.
- [63] O. Vinyals, C. Blundell, T. Lillicrap, D. Wierstra *et al.*, "Matching networks for one shot learning," *Advances in neural information processing systems*, vol. 29, pp. 3630–3638, 2016.
- [64] M. Ren, E. Triantafillou, S. Ravi, J. Snell, K. Swersky, J. B. Tenenbaum, H. Larochelle, and R. S. Zemel, "Meta-learning for semi-supervised few-shot classification," in *International Conference on Learning Representations ICLR*, 2018.
- [65] S. Ravi and H. Larochelle, "Optimization as a model for few-shot learning," in *International Conference on Learning Representations ICLR*, 2017.
- [66] S. Zagoruyko and N. Komodakis, "Wide residual networks," *arXiv preprint arXiv:1605.07146*, 2016.
- [67] Y. Wang, W.-L. Chao, K. Q. Weinberger, and L. van der Maaten, "Simpleshot: Revisiting nearest-neighbor classification for few-shot learning," *arXiv preprint arXiv:1911.04623*, 2019.



Florent Chiaroni received his Dipl.-Ing degree in computer science and electronics from ESTIA, France, in 2016, and his MSc in robotics and embedded systems from the University of Salford Manchester, United Kingdom, in the same year. He earned his Ph.D. in signal and image processing from the University of Paris Saclay in 2020, with VEDECOM Institute, Versailles, France, and Université Paris-Saclay, Centre national de la recherche scientifique (CNRS), CentraleSupélec, Gif-Sur-Yvette, France. He during the course of

this research, was a Postdoctoral Fellow at ÉTS Montréal, Canada and Institut National de la Recherche Scientifique (INRS), Montréal, Canada. He is currently a Research Scientist at Thales Research and Technology (TRT) Canada, Thales Digital Solutions (TDS), CortAIx, Montréal, Canada. His current research interests include civil unmanned aerial vehicles (UAVs) and efficient weakly-supervised learning for visual pattern analysis.



Malik Boudiaf obtained his MSc in Aeronautics & Astronautics from Stanford University in 2019, and his M.Eng in Aerospace Engineering from ISAE-Supaero, France in 2017, and his PhD degree from ÉTS Montréal, Canada, supervised by Prof. Ismail Ben Ayed and Prof. Pablo Piantanida. His research lies between Computer Vision, Information Theory, Optimization, and their application to few-shot/unsupervised learning. He is currently a Senior Machine Learning Engineer in Computer Vision and Natural Language Processing at Stealth Startup, Montréal, Canada.



Amar Mitiche holds the Licence Es Sciences degree in mathematics from the University of Algiers and the Ph.D. degree in computer science from the University of Texas at Austin. He is currently a Professor with the Department of Telecommunications (INRS-EMT), Institut National de la Recherche Scientifique (INRS), Montréal, QC, Canada. His research is in computer vision and pattern recognition. He has written several articles on the subjects, as well as three books: Computational Analysis of Visual Motion (Plenum Press, 1994), Variational and Level Set Methods in Image Segmentation (Springer, 2011), with Ismail Ben Ayed, and Computer Vision Analysis of Image Motion by Variational Methods (Springer, 2014), with J. K. Aggarwal. His current interests include image segmentation, image motion analysis, and pattern classification by neural networks.



Ismail Ben Ayed is currently a Full Professor at ÉTS Montréal. He is also affiliated with the CRCHUM. His interests are in computer vision, optimization, machine learning, and medical image analysis algorithms. Ismail authored over 100 fully peer-reviewed papers, mostly published in the top venues of those areas, along with 2 books and 7 US patents. In recent years, he gave over 30 invited talks, including 4 tutorials at flagship conferences (MICCAI'14, ISBI'16, MICCAI'19 and MICCAI'20). His research has been covered in several visible media outlets, such as Radio Canada (CBC), Quebec Science Magazine and Canal du Savoir. His research team received several recent distinctions, such as the MIDL'19 best paper runner-up award and several top-ranking positions in internationally visible contests. Ismail served as Program Committee for MICCAI'15, MICCAI'17 and MICCAI'19, and as Program Chair for MIDL'20. Also, he regularly serves as a reviewer for the main scientific journals of his field and was selected several times among the top reviewers of prestigious conferences (such as CVPR'15 and NEURIPS'20).

APPENDIX A

S_BETA COMPLEMENTARY DETAILS

We provide in this section the demonstrations for the mean, the variance, the mode, and parameter estimation of the presented s_Beta density function. Table 10 summarizes the resulting properties.

A.1 Mean and Variance

The mean of the probability density function $f(x)$ is defined as $E[X] = \int x f(x) dx$. Meanwhile, the variance of $f(x)$ can be defined as $V = E[X^2] - E[X]^2$ with $E[X^2] = \int x^2 f(x) dx$. Based on these two statements, we propose to estimate the mean and the variance of the proposed s_Beta density function $f_{s\text{Beta}}$.

s_Beta mean: To express the first moment $E_{sB}[X]$ of s_Beta, as a function its parameters, we propose to replace x with $(x + \delta - \delta)$ as follow:

$$\begin{aligned}
 E_{sB}[X] &= \int x f_{s\text{Beta}}(x) dx \\
 &= \int x \frac{(x + \delta)^{\alpha-1} (1 + \delta - x)^{\beta-1}}{B(\alpha, \beta) (1 + 2\delta)^{\alpha+\beta-2}} dx \\
 &\quad \text{replaces } x \\
 &= \int \frac{(x + \delta - \delta)(x + \delta)^{\alpha-1} (1 + \delta - x)^{\beta-1}}{B(\alpha, \beta) (1 + 2\delta)^{\alpha+\beta-2}} dx \\
 &= \frac{1}{B(\alpha, \beta) (1 + 2\delta)^{\alpha+\beta-2}} \times \\
 &\quad \int (x + \delta)^{(\alpha+1)-1} (1 + \delta - x)^{\beta-1} \\
 &\quad - \delta (x + \delta)^{\alpha-1} (1 + \delta - x)^{\beta-1} dx \\
 &= \frac{1}{B(\alpha, \beta) (1 + 2\delta)^{\alpha+\beta-2}} \times \\
 &\quad \int (x + \delta)^{(\alpha+1)-1} (1 + \delta - x)^{\beta-1} dx \\
 &\quad - \delta \int \frac{(x + \delta)^{\alpha-1} (1 + \delta - x)^{\beta-1}}{B(\alpha, \beta) (1 + 2\delta)^{\alpha+\beta-2}} dx \\
 &\quad \text{= } f_{s\text{Beta}}, \text{ so it integrates to 1} \\
 &= \frac{1}{B(\alpha, \beta) (1 + 2\delta)^{\alpha+\beta-2}} \times \\
 &\quad \int (x + \delta)^{(\alpha+1)-1} (1 + \delta - x)^{\beta-1} dx - \delta \\
 &= \frac{B(\alpha + 1, \beta) (1 + 2\delta)^{(\alpha+1)+\beta-2}}{B(\alpha, \beta) (1 + 2\delta)^{\alpha+\beta-2}} \times \\
 &\quad \int \frac{(x + \delta)^{(\alpha+1)-1} (1 + \delta - x)^{\beta-1}}{B(\alpha + 1, \beta) (1 + 2\delta)^{(\alpha+1)+\beta-2}} dx - \delta \\
 &\quad \text{= 1} \\
 &= \frac{B(\alpha + 1, \beta) (1 + 2\delta)}{B(\alpha, \beta)} - \delta,
 \end{aligned} \tag{23}$$

with $B(z_1, z_2) = \frac{\Gamma(z_1)\Gamma(z_2)}{\Gamma(z_1+z_2)}$. Then, with respect to the

property $\Gamma(z + 1) = z\Gamma(z)$, we have:

$$\begin{aligned}
 E_{sB}[X] &= \frac{\Gamma(\alpha + 1)\Gamma(\beta)\Gamma(\alpha + \beta)}{\Gamma(\alpha + 1 + \beta)\Gamma(\alpha)\Gamma(\beta)} (1 + 2\delta) - \delta \\
 &= \frac{\Gamma(\alpha + 1)\Gamma(\alpha + \beta)}{\Gamma(\alpha + 1 + \beta)\Gamma(\alpha)} (1 + 2\delta) - \delta \\
 &= \frac{\alpha\Gamma(\alpha)\Gamma(\alpha + \beta)}{(\alpha + \beta)\Gamma(\alpha + \beta)\Gamma(\alpha)} (1 + 2\delta) - \delta \\
 &= \frac{\alpha}{\alpha + \beta} (1 + 2\delta) - \delta.
 \end{aligned} \tag{24}$$

s_Beta variance: We first estimate the second moment $E_{sB}[X^2]$ by replacing x^2 with $(x + \delta - \delta)^2 = (x + \delta)^2 - 2\delta(x + \delta) + \delta^2$ as follow:

$$\begin{aligned}
 E_{sB}[X^2] &= \int x^2 f_{s\text{Beta}}(x) dx \\
 &= \int (x + \delta - \delta)^2 f_{s\text{Beta}}(x) dx \\
 &= \int ((x + \delta)^2 - 2\delta(x + \delta) + \delta^2) f_{s\text{Beta}}(x) dx \\
 &= \int (x + \delta)^2 f_{s\text{Beta}}(x) dx - 2\delta \int (x + \delta) f_{s\text{Beta}}(x) dx \\
 &\quad + \delta^2 \underbrace{\int f_{s\text{Beta}}(x) dx}_{=1} \\
 &= \underbrace{\frac{(\alpha + 1)\alpha}{(\alpha + 1 + \beta)(\alpha + \beta)} (1 + 2\delta)^2 - 2\delta \frac{\alpha}{\alpha + \beta} (1 + 2\delta) + \delta^2}_{\text{Using Eq. (26)}} \underbrace{+ \delta^2}_{\text{Using Eq. (27)}}
 \end{aligned} \tag{25}$$

The term $\int (x + \delta)^2 f_{s\text{Beta}}(x) dx$ from Eq. (25) can be developed as:

$$\begin{aligned}
 &\int (x + \delta)^2 f_{s\text{Beta}}(x) dx \\
 &= \int (x + \delta)^2 \frac{(x + \delta)^{\alpha-1} (1 + \delta - x)^{\beta-1}}{B(\alpha, \beta) (1 + 2\delta)^{\alpha+\beta-2}} dx \\
 &= \frac{1}{B(\alpha, \beta) (1 + 2\delta)^{\alpha+\beta-2}} \times \\
 &\quad \int (x + \delta)^{(\alpha+2)-1} (1 + \delta - x)^{\beta-1} dx \\
 &= \frac{B(\alpha + 2, \beta) (1 + 2\delta)^{(\alpha+2)+\beta-2}}{B(\alpha, \beta) (1 + 2\delta)^{\alpha+\beta-2}} \times \\
 &\quad \int \frac{(x + \delta)^{(\alpha+2)-1} (1 + \delta - x)^{\beta-1}}{B(\alpha + 2, \beta) (1 + 2\delta)^{(\alpha+2)+\beta-2}} dx \\
 &\quad \text{= 1} \\
 &= \frac{B(\alpha + 2, \beta) (1 + 2\delta)^{(\alpha+\beta-2)+2}}{B(\alpha, \beta) (1 + 2\delta)^{\alpha+\beta-2}} \\
 &= B(\alpha + 2, \beta) \frac{1}{B(\alpha, \beta)} (1 + 2\delta)^2 \\
 &= \frac{\Gamma(\alpha + 2)\Gamma(\beta)}{\Gamma(\alpha + 2 + \beta)} \frac{\Gamma(\alpha + \beta)}{\Gamma(\alpha)\Gamma(\beta)} (1 + 2\delta)^2 \\
 &= \frac{(\alpha + 1)\alpha\Gamma(\alpha)\Gamma(\beta)\Gamma(\alpha + \beta)}{(\alpha + 1 + \beta)(\alpha + \beta)\Gamma(\alpha + \beta)\Gamma(\alpha)\Gamma(\beta)} (1 + 2\delta)^2 \\
 &= \frac{(\alpha + 1)\alpha}{(\alpha + 1 + \beta)(\alpha + \beta)} (1 + 2\delta)^2.
 \end{aligned} \tag{26}$$

TABLE 10: sBeta and related Beta properties depending on their respective probability density function.

	sBETA	BETA
DENSITY FUNCTION	$f_{\text{sBeta}} = \frac{(x + \delta)^{\alpha-1}(1 + \delta - x)^{\beta-1}}{B(\alpha, \beta)(1 + 2\delta)^{\alpha+\beta-2}}$	$f_{\text{Beta}} = \frac{x^{\alpha-1}(1 - x)^{\beta-1}}{B(\alpha, \beta)}$
MEAN (SEC. A.1)	$E_{sB}[X] = \frac{\alpha}{\alpha + \beta}(1 + 2\delta) - \delta$	$E_B[X] = \frac{\alpha}{(\alpha + \beta)}$
VARIANCE (SEC. A.1)	$V_{sB}[X] = \frac{\alpha\beta}{(\alpha + \beta)^2(\alpha + \beta + 1)}(1 + 2\delta)^2$	$V_B[X] = \frac{\alpha\beta}{(\alpha + \beta)^2(\alpha + \beta + 1)}$
MODE (SEC. A.2)	$m_{sB} = \frac{\alpha - 1 + \delta(\alpha - \beta)}{\alpha + \beta - 2}$	$m_B = \frac{\alpha - 1}{\alpha + \beta - 2}$
CONCENTRATION (SEC. 4.2.3)	$\lambda = \alpha + \beta - 2$	$\lambda = \alpha + \beta - 2$
METHOD OF MOMENTS (SEC. 4.3)	$\alpha = \left(\frac{\mu_\delta(1 - \mu_\delta)(1 + 2\delta)^2}{V_{sB}[X]} - 1\right)\mu_\delta$ $\beta = \left(\frac{\mu_\delta(1 - \mu_\delta)(1 + 2\delta)^2}{V_{sB}[X]} - 1\right)(1 - \mu_\delta),$ WITH $\mu_\delta = \frac{E_{sB}[X] + \delta}{1 + 2\delta}$	$\alpha = \left(\frac{E_B[X](1 - E_B[X])}{V_B[X]} - 1\right)E_B[X]$ $\beta = \left(\frac{E_B[X](1 - E_B[X])}{V_B[X]} - 1\right)(1 - E_B[X])$

Similarly, the term $-2\delta \int (x + \delta) f_{\text{sBeta}}(x) dx$ from Eq. (25) can be developed as:

$$\begin{aligned}
 -2\delta \int (x + \delta) f_{\text{sBeta}}(x) dx \\
 &= -2\delta \int \underbrace{\frac{(x + \delta)^{(\alpha+1)-1}(1 + \delta - x)^{\beta-1}}{B(\alpha, \beta)(1 + 2\delta)^{\alpha+\beta-2}} dx}_{=E_{sB}[X]+\delta=\frac{\alpha}{\alpha+\beta}(1+2\delta) \text{ using Eq. (23)}} \\
 &= -2\delta \frac{\alpha}{\alpha + \beta}(1 + 2\delta).
 \end{aligned} \tag{27}$$

Finally, we can estimate the variance (i.e., the second central moment) $V_{sB}[X]$, as a function of sBeta density parameters, using Eq. (23) and Eq. (25) as follow:

$$\begin{aligned}
 V_{sB}[X] &= E_{sB}[X^2] - E_{sB}[X]^2 \\
 &= \frac{(\alpha + 1)\alpha}{(\alpha + 1 + \beta)(\alpha + \beta)}(1 + 2\delta)^2 \\
 &\quad - 2\delta \frac{\alpha}{\alpha + \beta}(1 + 2\delta) + \delta^2 \\
 &\quad - \left[\frac{\alpha}{\alpha + \beta}(1 + 2\delta) - \delta \right]^2 \\
 &= \frac{\alpha\beta}{(\alpha + \beta)^2(\alpha + \beta + 1)}(1 + 2\delta)^2.
 \end{aligned} \tag{28}$$

Linear property: With respect to the expectation linearity, it is worth noting that we have $\frac{E[X]+\delta}{1+2\delta} = E\left[\frac{X+\delta}{1+2\delta}\right]$ and

$$\begin{aligned}
 V\left[\frac{X + \delta}{1 + 2\delta}\right] &= E\left[\left(\frac{X + \delta}{1 + 2\delta} - E\left[\frac{X + \delta}{1 + 2\delta}\right]\right)^2\right] \\
 &= \frac{E[(X - E[X])^2]}{(1 + 2\delta)^2} \\
 &= \frac{V[X]}{(1 + 2\delta)^2}.
 \end{aligned} \tag{29}$$

A.2 Mode

The mode of a density function $f(x)$ corresponds to the value of x at which $f(x)$ achieves its maximum.

sBeta mode: To find the mode of sBeta depending on α and β parameters, we estimate at which value of x the derivative of f_{sBeta} is equal to 0. We first estimate the derivative as follows:

$$\begin{aligned}
 f'_{\text{sBeta}}(x) &= \frac{df_{\text{sBeta}}(x)}{dx} = \frac{d}{dx} \frac{(x + \delta)^{\alpha-1}(1 + \delta - x)^{\beta-1}}{B(\alpha, \beta)(1 + 2\delta)^{\alpha+\beta-2}} \\
 &= \frac{1}{B(\alpha, \beta)(1 + 2\delta)^{\alpha+\beta-2}} \frac{d}{dx} (x + \delta)^{\alpha-1}(1 + \delta - x)^{\beta-1} \\
 &= \frac{(\alpha - 1)(x + \delta)^{\alpha-2}(1 + \delta - x)^{\beta-1}}{B(\alpha, \beta)(1 + 2\delta)^{\alpha+\beta-2}} \\
 &\quad - \frac{(x + \delta)^{\alpha-1}(\beta - 1)(1 + \delta - x)^{\beta-2}}{B(\alpha, \beta)(1 + 2\delta)^{\alpha+\beta-2}}.
 \end{aligned} \tag{30}$$

Then, we can solve $\frac{df_{\text{sBeta}}(x)}{dx} = 0$ as follow:

$$\begin{aligned}
 \frac{df_{\text{sBeta}}(x)}{dx} &= 0 \\
 \Rightarrow (\alpha - 1)(x + \delta)^{\alpha-2}(1 + \delta - x)^{\beta-1} \\
 &\quad - (x + \delta)^{\alpha-1}(\beta - 1)(1 + \delta - x)^{\beta-2} = 0 \\
 \Rightarrow (\alpha - 1)(1 + \delta - x) - (\beta - 1)(x + \delta) &= 0 \\
 \Rightarrow x &= \frac{\alpha - 1 + \delta(\alpha - \beta)}{\alpha + \beta - 2}.
 \end{aligned} \tag{31}$$

Thus, the mode of sBeta with $\alpha, \beta > 1$ is defined as $m_{sB} = \frac{\alpha - 1 + \delta(\alpha - \beta)}{\alpha + \beta - 2}$.

A.3 Solving the necessary conditions for minimizing the objective w.r.t sBeta parameters

Let us compute the partial derivatives of our objective L_{sBeta} (14) for $\alpha_{k,n}$ and $\beta_{k,n}$:

$$\begin{aligned} \frac{\partial L_{\text{sBeta}}}{\partial \alpha_{k,n}} &= \sum_{i=1}^N u_{i,k} \log(x_{i,n} + \delta) - \left(\sum_{i=1}^N u_{i,k} \right) \log(1 + 2\delta) \\ &\quad - \left(\sum_{i=1}^N u_{i,k} \right) (\psi(\alpha_{k,n}) - \psi(\alpha_{k,n} + \beta_{k,n})) \\ \frac{\partial L_{\text{sBeta}}}{\partial \beta_{k,n}} &= \sum_{i=1}^N u_{i,k} \log(1 + \delta - x_{i,n}) - \left(\sum_{i=1}^N u_{i,k} \right) \log(1 + 2\delta) \\ &\quad - \left(\sum_{i=1}^N u_{i,k} \right) (\psi(\beta_{k,n}) - \psi(\alpha_{k,n} + \beta_{k,n})) \end{aligned} \quad (32)$$

where ψ stands for the di-gamma function. Setting partial derivatives in (32) to 0 leads to the following coupled system:

$$\begin{aligned} \alpha_{k,n} &= \psi^{-1}(\psi(\alpha_{k,n} + \beta_{k,n}) \\ &\quad + \frac{1}{\sum_{i=1}^N u_{i,k}} \sum_{i=1}^N u_{i,k} \log(\frac{x_{i,n} + \delta}{1 + 2\delta})) \\ \beta_{k,n} &= \psi^{-1}(\psi(\alpha_{k,n} + \beta_{k,n}) \\ &\quad + \frac{1}{\sum_{i=1}^N u_{i,k}} \sum_{i=1}^N u_{i,k} \log(\frac{1 + \delta - x_{i,n}}{1 + 2\delta})) \end{aligned} \quad (33)$$

While (33) does not have any analytical solution, we approximate updates in (33) by fixing the right-hand side of each equation, leading the following vectorized updates of parameters α_k and β_k for each cluster k :

$$\alpha_k^{(t+1)} = \psi^{-1}(\psi(\alpha_k^{(t)} + \beta_k^{(t)}) \quad (34)$$

$$+ \frac{1}{\sum_{i=1}^N u_{i,k}} \sum_{i=1}^N u_{i,k} \log(\frac{x_i + \delta}{1 + 2\delta})) \quad (35)$$

$$\beta_k^{(t+1)} = \psi^{-1}(\psi(\alpha_k^{(t)} + \beta_k^{(t)}) \quad (36)$$

$$+ \frac{1}{\sum_{i=1}^N u_{i,k}} \sum_{i=1}^N u_{i,k} \log(\frac{1 + \delta - x_i}{1 + 2\delta}))$$

We empirically validated such optimization procedure converged to the MLE estimate on the synthetically generated dataset.

APPENDIX B SUPPLEMENTARY EXPERIMENTS

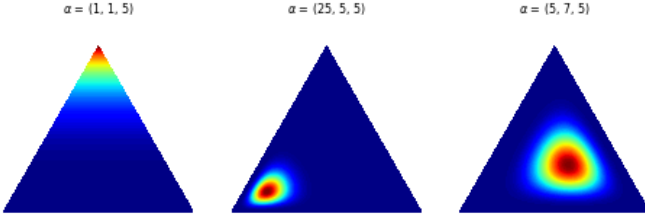


Fig. 7: Visualization on Δ^2 of the three Dirichlet distributions used to generate random artificial datasets *Simu* and *iSimus*, introduced in Sec. 5.

TABLE 11: Balanced clustering on *Simu* depending on the dataset size.

DATASET SIZE APPROACH	100 000 (NMI)	10 000 (NMI)	1 000 (NMI)	100 (NMI)
ARGMAX	60.1 ± 0.5	59.8 ± 0.7	60.4 ± 3.9	62.0 ± 17.9
K-MEANS	76.6 ± 0.1	76.7 ± 0.5	76.9 ± 6.2	78.2 ± 21.8
KL K-MEANS	76.2 ± 0.2	76.3 ± 0.7	76.5 ± 6.2	78.1 ± 22.8
GMM	75.8 ± 0.3	75.8 ± 1.2	75.9 ± 6.8	77.3 ± 28.4
K-MEDIANS	76.8 ± 0.1	77.1 ± 0.7	77.1 ± 5.6	78.7 ± 22.2
K-MEDOIDS	60.8 ± 14.4	64.2 ± 12.1	65.3 ± 19.4	71.8 ± 24.2
K-MODES	76.2 ± 0.2	76.3 ± 1.0	76.5 ± 5.3	77.5 ± 24.9
HSC	9.3 ± 1.9	15.0 ± 2.7	30.6 ± 16.3	41.2 ± 27.9
K-SBETAS	79.5 ± 0.1	79.5 ± 0.8	79.8 ± 6.4	80.0 ± 25.4

TABLE 12: Imbalanced clustering on *iSimus* depending on the dataset size.

DATASET SIZE APPROACH	100 000 (NMI)	10 000 (NMI)	1 000 (NMI)
ARGMAX	55.5 ± 25.5	55.6 ± 26.8	55.6 ± 31.5
K-MEANS	62.3 ± 22.6	62.2 ± 23.4	62.4 ± 28.9
KL K-MEANS	59.9 ± 25.2	59.9 ± 26.0	60.2 ± 31.5
GMM	60.6 ± 23.9	63.8 ± 29.3	63.9 ± 35.0
K-MEDIANS	60.4 ± 24.8	60.3 ± 25.6	60.3 ± 32.2
K-MEDOIDS	47.2 ± 33.0	55.4 ± 30.0	57.8 ± 35.9
K-MODES	55.1 ± 30.9	54.9 ± 32.4	54.8 ± 36.5
HSC	17.7 ± 12.1	13.6 ± 11.7	29.1 ± 31.8
K-SBETAS	72.4 ± 17.2	72.2 ± 20.1	73.3 ± 29.2

TABLE 13: **Running time** of K-SBETAS (GPU-based) on *GTA5 road* → *Cityscapes road* depending on the subset size. This GPU-based implementation uses the pytorch library. We fixed to 10 the maximum number of K-SBETAS clustering iterations. We assume that the segmentation model and K-SBETAS method run on the same GPU, i.e., no loading time is implied by the softmax prediction set. The CPU used is 11th Gen Intel(R) Core(TM) i7-11700K 3.60GHz. GPU used: NVIDIA GeForce RTX 2070 SUPER. Presented prediction scores were all obtained on the full-size (1024*2048) set.

SUBSET SIZE	RUNNING TIME (SECONDS)		FULL SIZE SCORES	
	(CLUSTERING)	(PREDICTION)	(NMI)	(MIoU)
FULL SIZE (1024*2048)	0.2784	0.0056	35.8	65.7
MODULO 2 (512*1024)	0.0812	0.0019	35.8	65.7
MODULO 4 (256*512)	0.0282	0.0009	35.8	65.7
MODULO 8 (128*256)	0.0165	0.0004	35.8	65.7

TABLE 14: **k-means++** versus **vertex init** (proposed). Balanced clustering on softmax predictions. Performances are averaged over ten executions. Note that k-means++ is stochastic while the vertex init is not.

DATASET	SVHN → MNIST		VISDA-C	
	K-MEANS++ (ACC)	VERTEX INIT (ACC)	K-MEANS++ (ACC)	VERTEX INIT (ACC)
K-MEANS	66.6 ± 5.4	68.9 ± 0.0	44.5 ± 3.3	47.9 ± 0.0
KL K-MEANS	72.6 ± 7.8	75.5 ± 0.0	50.0 ± 2.7	51.2 ± 0.0
GMM	60.6 ± 9.6	69.2 ± 0.0	43.8 ± 5.2	49.4 ± 0.0
K-MEDIANS	67.4 ± 9.2	68.8 ± 0.0	38.5 ± 4.0	40.0 ± 0.0
K-MEDOIDS	51.9 ± 4.9	71.3 ± 0.0	40.6 ± 8.6	46.8 ± 0.0
K-MODES	60.6 ± 13.0	71.3 ± 0.0	30.2 ± 6.3	31.1 ± 0.0
K-SBETAS	69.8 ± 8.1	76.6 ± 0.0	47.2 ± 5.2	56.0 ± 0.0

B.0.1 One-Shot Learning

TABLE 15: **1-shot plug-in results.** The proposed K-SBETAS further boosts results of existing One-Shot methods by clustering their soft predictions on the query set.

METHOD	NETWORK	miniIMAGENET		tieredIMAGENET	
		(NMI)	(ACC)	(NMI)	(ACC)
SIMPLESHOT	RN-18	49.1	62.7	57.5	69.2
SIMPLESHOT + K-SBETAS	RN-18	52.2	64.4	60.5	71.0
BD-CSPN	RN-18	58.2	68.9	67.2	76.0
BD-CSPN + K-SBETAS	RN-18	60.5	69.8	68.9	76.6
SIMPLESHOT	WRN-28-10	53.6	65.7	59.1	70.4
SIMPLESHOT + K-SBETAS	WRN-28-10	56.8	67.3	61.8	72.4
BD-CSPN	WRN-28-10	62.4	72.1	69.0	77.5
BD-CSPN + K-SBETAS	WRN-28-10	64.0	72.4	70.7	78.3

We consider the One-Shot classification problem, in which a model is evaluated based on its ability to generalize to new classes from a single labeled example per class. Typically, One-Shot methods use the labeled support set S of each task to build a classifier and obtain soft predictions for unlabelled query samples. Once soft predictions have been obtained, proposed K-SBETAS can be used to further refine predictions by clustering soft predictions of the entire query set.

Setup. We use two standard benchmarks for One-Shot classification: *mini-Imagenet* [63] and *tiered-Imagenet* [64]. The *mini-Imagenet* benchmark is composed of 60,000 color images [63] equally split among 100 classes, themselves split between train, val, and test following [65]. The *tiered-Imagenet* benchmark is a larger dataset with 779,165 images and 608 classes, split following [64]. All images are resized to 84×84 . Regarding the networks, we use the pre-trained RN-18 [41] and WRN28-10 [66] provided by [53]. Only 15 unlabeled query data points per class are available during each separate task, so we use the biased version of K-SBETAS. As for the methods, we select one inductive method: SimpleSHOT [67] and one transductive method: BD-CSPN [51]. Each One-Shot method is reproduced using the set of hyperparameters suggested in the original papers.

Results. Table 15 shows that all along these experiments, K-SBETAS consistently improves in terms of NMI and Accuracy scores the output predictions of SimpleSHOT and BD-CSPN.

TABLE 16: **iVISDA-Cs imbalanced proportions.** To obtain 10 imbalanced subsets of VISDA-C that we refer to *iVISDA-Cs*, we have randomly generated ten random vectors from a Dirichlet distribution. VISDA-C contains 12 classes, so the dimension of this Dirichlet distribution is equal to 12. Dirichlet parameters are set as $\alpha = \{\alpha_n = 1\}_{n=1}^{D=12}$, such that this dirichlet distribution is uniform on Δ^{11} . Below is the list of the ten sets of rounded proportions obtained and the corresponding number of examples for each VISDA-C class. For every class, examples from the original dataset are always picked in the same order, starting at the beginning of the target image list of VISDA-C.

CLASSES	PLANE	BCYCL	BUS	CAR	HORSE	KNIFE	MCYCL	PERSON	PLANT	SKTBRD	TRAIN	TRUCK
VISDA-C PROPORTIONS	0.0658	0.0627	0.0847	0.1878	0.0847	0.0375	0.1046	0.0722	0.0821	0.0412	0.0765	0.1002
NUMBER OF EXAMPLES	3646	3475	4690	10401	4691	2075	5796	4000	4549	2281	4236	5548
PROPORTIONS SET 1	0.0406	0.2315	0.0953	0.0257	0.2367	0.0443	0.0930	0.0252	0.1347	0.0601	0.0012	0.0116
NUMBER OF EXAMPLES	275	1568	645	173	1603	300	630	170	912	407	8	78
PROPORTIONS SET 2	0.0996	0.0234	0.0086	0.0112	0.1490	0.0064	0.1900	0.1223	0.1287	0.0387	0.0876	0.1346
NUMBER OF EXAMPLES	675	158	58	75	1009	43	1286	828	871	262	593	912
PROPORTIONS SET 3	0.0511	0.1170	0.0779	0.0661	0.0127	0.0575	0.0166	0.1958	0.0047	0.0795	0.2147	0.1064
NUMBER OF EXAMPLES	346	792	527	448	85	389	112	1326	31	538	1454	720
PROPORTIONS SET 4	0.1382	0.0014	0.1726	0.0017	0.0030	0.1600	0.2470	0.0726	0.0419	0.0524	0.0558	0.0534
NUMBER OF EXAMPLES	936	9	1169	11	20	1084	1673	492	284	354	378	361
PROPORTIONS SET 5	0.0013	0.0227	0.1451	0.1049	0.2725	0.0511	0.0196	0.0500	0.1401	0.0193	0.0322	0.1411
NUMBER OF EXAMPLES	8	154	983	710	1846	346	132	338	948	130	218	956
PROPORTIONS SET 6	0.1450	0.0202	0.0343	0.1604	0.0574	0.0183	0.0318	0.0368	0.2668	0.0356	0.1361	0.0570
NUMBER OF EXAMPLES	982	137	232	1086	388	123	215	249	1807	241	922	386
PROPORTIONS SET 7	0.1200	0.1304	0.0310	0.0451	0.0308	0.0071	0.1194	0.2701	0.0122	0.1311	0.0911	0.0116
NUMBER OF EXAMPLES	812	883	209	305	208	48	809	1830	82	888	617	78
PROPORTIONS SET 8	0.0166	0.0521	0.0457	0.0358	0.1175	0.1917	0.0258	0.2303	0.1503	0.0379	0.0600	0.0362
NUMBER OF EXAMPLES	112	352	309	242	796	1298	174	1560	1018	256	406	245
PROPORTIONS SET 9	0.1523	0.1316	0.0196	0.0427	0.0380	0.0806	0.0423	0.2075	0.0383	0.0644	0.1074	0.0754
NUMBER OF EXAMPLES	1031	891	132	289	257	546	286	1405	259	436	727	510
PROPORTIONS SET 10	0.0102	0.1336	0.0063	0.0131	0.1291	0.0812	0.0019	0.0967	0.3063	0.0770	0.1107	0.0337
NUMBER OF EXAMPLES	69	905	42	88	874	549	12	655	2074	521	750	228

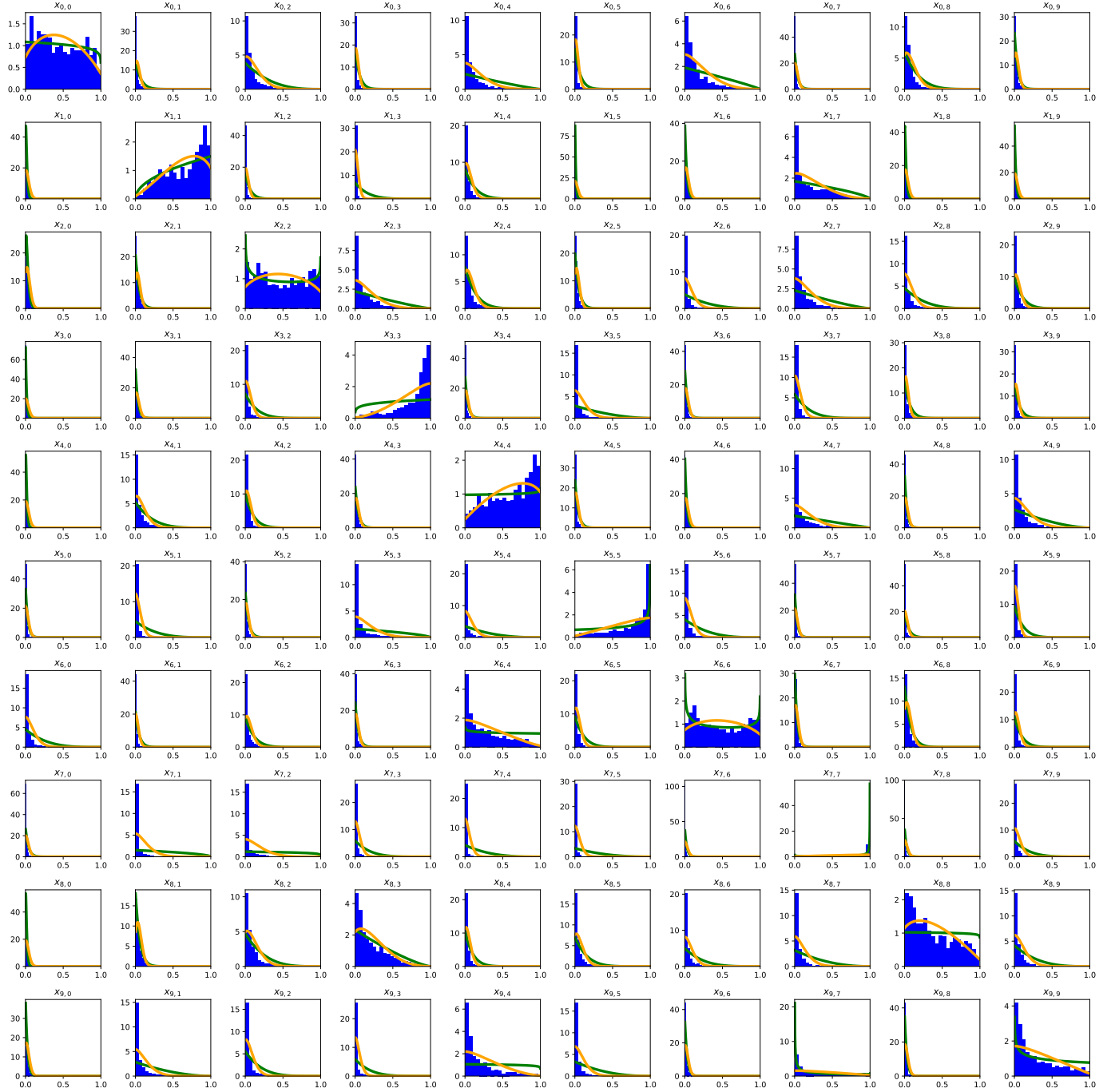


Fig. 8: Histograms per coordinate of softmax predictions obtained on MNIST, with a source model pre-trained on SVHN. Rows correspond to softmax predictions for a given class. Columns refer to the softmax prediction coordinates. Green curves represent Beta density estimations, and orange curves represent sBeta density estimations. *We invite the reader on the pdf version to zoom on these vectorized figures.*

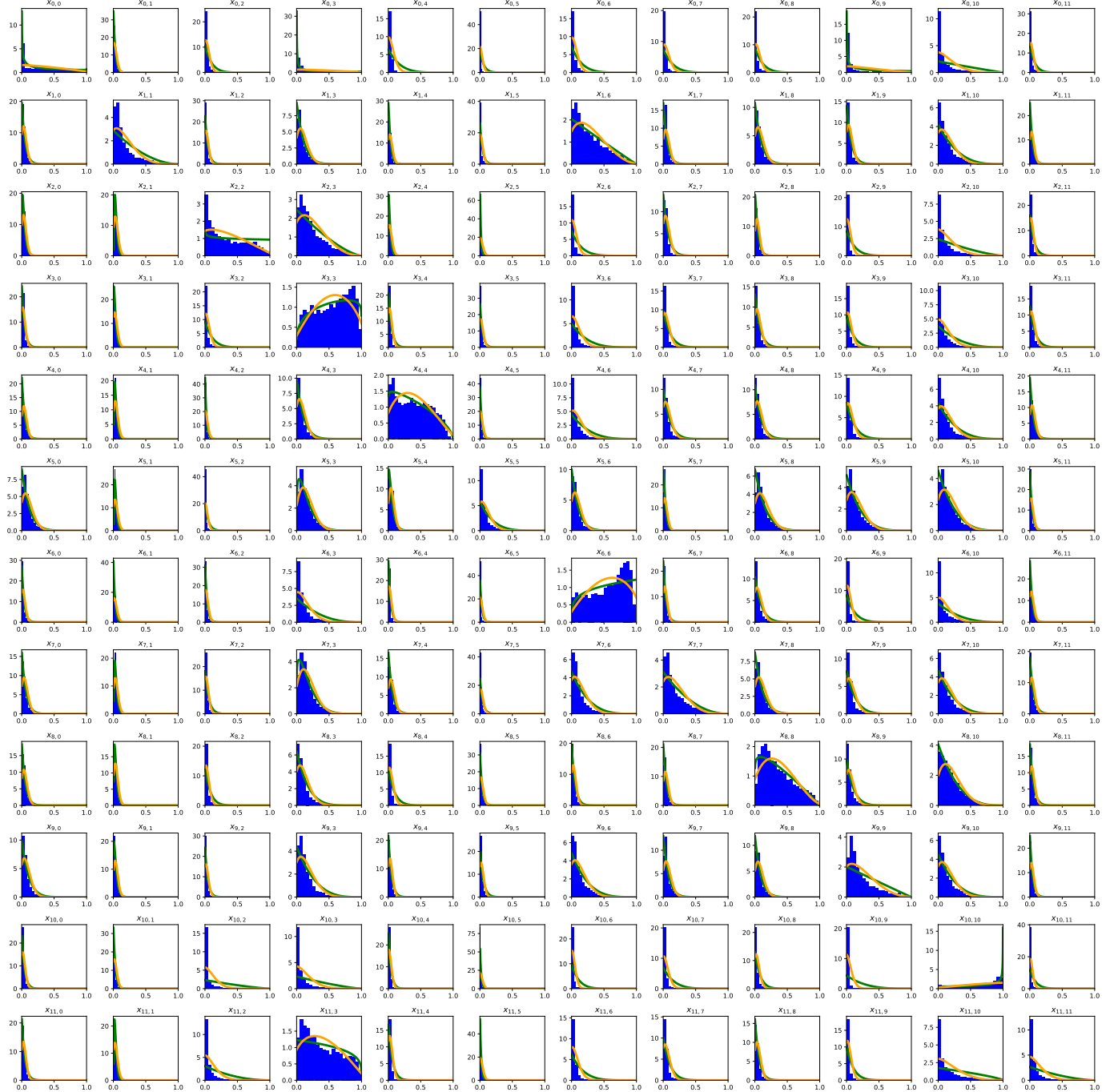


Fig. 9: Histograms per coordinate of softmax predictions on the challenge VISDA-C. Rows correspond to softmax predictions for a given class. Columns refer to softmax prediction coordinates. Green curves represent Beta density estimations, and orange curves represent sBeta density estimations. *We invite the reader on the pdf version to zoom on these vectorized figures.*